UNIVERSIDADE FEDERAL DE ALFENAS

FELIPE TERRA MARTINS

ESTUDO CRISTALOQUÍMICO DE BENZOFENONAS PRENILADAS EXTRAÍDAS DE SEMENTES E FRUTOS DE *RHEEDIA BRASILIENSIS*: ESTRUTURA CRISTALINA E RELAÇÃO ESTRUTURA–ATIVIDADE

Alfenas/MG

2008

FELIPE TERRA MARTINS

ESTUDO CRISTALOQUÍMICO DE BENZOFENONAS PRENILADAS EXTRAÍDAS DE SEMENTES E FRUTOS DE *RHEEDIA BRASILIENSIS*: ESTRUTURA CRISTALINA E RELAÇÃO ESTRUTURA–ATIVIDADE

Dissertação apresentada como parte dos requisitos para obtenção do título de Mestre em Ciências Farmacêuticas pela Universidade Federal de Alfenas. Área de concentração: Avaliação físico-química e microbiológica de fármacos e medicamentos.
Orientador: Antônio Carlos Doriguetto.

Alfenas/MG
2008

FELIPE TERRA MARTINS

ESTUDO CRISTALOQUÍMICO DE BENZOFENONAS PRENILADAS EXTRAÍDAS DE SEMENTES E FRUTOS DE *RHEEDIA BRASILIENSIS*: ESTRUTURA CRISTALINA E RELAÇÃO ESTRUTURA–ATIVIDADE

A Banca examinadora abaixo-assinada aprova a Dissertação apresentada como parte dos requisitos para obtenção do título de Mestre em Ciências Farmacêuticas pela Universidade Federal de Alfenas. Área de concentração: Avaliação físico-química e microbiológica de fármacos e medicamentos.

Aprovada em:

Profº. Dr. Nelson Gonçalves Fernandes
Departamento de Química, Instituto de Ciências Exatas, UFMG
Assinatura:

Profº. Dr. Carlos Henrique Tomich de Paula da Silva
Faculdade de Ciências Farmacêuticas de Ribeirão Preto, Universidade de São Paulo - FCFRP/USP
Assinatura:

Profº. Dr. Antônio Carlos Doriguetto
Departamento de Ciências Exatas, UNIFAL-MG
Asinatura:

AGRADECIMENTOS

À Universidade Federal de Alfenas pela oportunidade oferecida.

Ao Prof. Dr. Antônio Carlos Doriguetto, orientador, pela dedicação, conhecimentos transmitidos e confiança depositada na realização deste trabalho.

Ao Prof. Dr. Marcelo Henrique dos Santos, co-orientador, pelo auxílio e amizade durante a realização deste trabalho.

Ao Prof. Luiz Claudio de Almeida Barbosa (Dep. Química - UFV), pela colaboração nas análises cromatográficas e de espectrometria de massas.

Ao Prof. Javier Ellena (IFSC-USP), por disponibilizar o Laboratório de Difração de raios X e o difratômetro de monocristal.

À Profa. Lira Celeste Alves e ao discente do curso de Farmácia Diego Magno Assis (UNIFAL-MG), pela parceria nos ensaios de avaliação da atividade enzimática.

À Profa. Maria Aparecida Juliano (Unifesp), por disponibilizar o espectrofluorímetro do Departamento de Biofísica, Unifesp.

Aos Prof. Ihosvany Camps e Profa. Márcia Paranho Veloso, pelo auxílio nos experimentos de modelagem computacional.

Aos jovens pesquisadores Thiago Correa de Souza e Priscilla Bento Matos Cruz, pelos esforços laboratoriais para isolamento e purificação dos produtos naturais.

À Coordenação do Curso de Pós-Graduação pela política de incentivo à produção acadêmica.

À Coordenação de Aperfeiçoamento de Pessoal de Nível Superior – CAPES pela bolsa de Mestrado concedida.

Aos amigos, minha eterna gratidão.

RESUMO

A presente dissertação de Mestrado é dividida em duas partes: a primeira, dedicada à obtenção de extratos das sementes e frutos de *Rheedia brasiliensis* Pl. & T para isolamento de benzofenonas polipreniladas bioativas e identificação de suas estruturas moleculares e cristalinas, contem dois artigos científicos acerca da elucidação estrutural, por técnicas espectroscópicas e cristalográficas, de dois produtos naturais, gutiferona A e garciniafenona; a segunda, por sua vez, é constituída de um artigo científico no qual é descrita a atividade inibitória dos dois compostos supracitados e de outras duas benzofenonas, epiclusianona, também isolada de *Rheedia brasiliensis*, e 2,2',4-triidroxibenzofenona, sintetizada através de substituição eletrofílica aromática, sobre quatro proteases: papaína, tripsina, catepsina B e catepsina G. Garciniafenona foi isolada pioneiramente dos frutos de *Rheedia brasiliensis* e sua completa caracterização é apresentada em um dos artigos supracitados. No outro, a estrutura cristalográfica de gutiferona A, uma benzofenona natural com propriedades inibitórias sobre a infecção por HIV e isolada pela primeira vez de *Symphonia globulifera*, é reportada. Em ambos os artigos, as estruturas de garciniafenona e gutiferona A são discutidas comparando os parâmetros geométricos, eletrônicos e estéricos determinados, com aqueles descritos na literatura para epiclusianona e o seu epímero, clusianona, esclarecendo relações entre configuração e tautomerismo ceto-enólico. O artigo relativo ao efeito inibitório das benzofenonas sobre proteases traz resultados experimentais que foram correlacionados com certos motivos estruturais cristalograficamente estimados, possibilitando o estabelecimento de relações entre as estruturas químicas dos compostos testados e a atividade anti-proteolítica, as quais são fortemente suportadas por ensaios computacionais de ancoragem dos inibidores no alvo macromolecular.

Palavras-chave: *Rheedia brasiliensis*. Benzofenonas polipreniladas. Gutiferona A. Garciniafenona. Cristalografia por difração de raios X. Atividade anti-proteolítica.

ABSTRACT

The present Master degree dissertation contains two parts: the first one, which was devoted to extract preparation from *Rheedia brasiliensis* seeds and fruits in order to isolate bioactive polyprenylated benzophenones and to identify their molecular and crystalline structures, leads two articles on structural elucidation of two natural products by X-ray crystallography and spectroscopic techniques: guttiferone A and garciniaphenone; the second one is a paper describing the inhibiting activity of the two compounds before mentioned and other two benzophenone-type derivatives, epiclusianone, which was also isolated from *Rheedia brasiliensis*, and 2,2',4-trihydroxybenzophenone, which was synthesized by aromatic electrophilic substitution, against four proteases, papain, trypsin, cathepsin B and cathepsin G. Garciniaphenone has been discovered for the first time in *Rheedia brasiliensis* fruits and its complete characterization is given on a paper of the series. The crystallographic structure of a HIV-inhibitory benzophenone that was initially isolated from *Symphonia globulifera*, guttiferone A, is reported on another article of the series. On both papers, the structures of garciniaphenone and guttiferone A are analyzed matching their steric, electronic and geometrical features to that found in the literature for epiclusianone and its epimer, clusianone, which has allowed to state relationships between configuration and keto-enol tautomerism. The article concerning the inhibiting effect of benzophenones on proteases shows experimental data that were correlated with certain structural motifs determined by X-ray diffraction crystallography, establishing structure-activity relationships strongly supported by theoretical investigations using computational docking to predict the inhibitor-enzyme complex interaction pattern.

Keywords: *Rheedia brasiliensis*. Polyprenylated benzophenones. Guttiferone A. Garciniaphenone. X-ray crystallography. Antiproteolytic activity.

SUMÁRIO

1 REVISÃO DA LITERATURA

1.1 FAMÍLIA GUTTIFERAE

A família Guttiferae Juss., também chamada, alternativamente, por Clusiaceae Lindl., engloba árvores, arbustos, ervas e lianas. São plantas de distribuição geográfica variando entre a zona temperada até a tropical, apresentando comportamentos auto-sustentáveis na maioria das vezes (Waterman, 1986). Algumas espécies são cianogênicas, com ausência ou raras presenças de alcalóides (Waterman, 1986). Em alguns gêneros existem heterosídeos antraquinônicos derivados de poliacetatos, apresentando também flavonóides, proantocianidinas, cianidinas, delfinidinas, quercetina, kaempferol e miricetina (Waterman, 1986).

Esta família é dotada de uma variedade de metabólitos biologicamente ativos, tais como as benzofenonas poli-isopreniladas (Gustafson et al., 1992; Williams et al., 2003). Do ponto de vista estrutural, compostos pertencentes a esta classe química apresentam obrigatoriamente um núcleo benzofenônico (difenilmetanona) substituído por grupo(s) isoprenila(s) (3-metil-2-butenila). Um padrão de oxigenação tríplice em um dos anéis aromáticos do cerne difenilmetanona acompanhada por uma ciclização intramolecular adicional, a qual origina um sistema bicíclico de nove átomos de carbono, também pode ser descrito para a maioria dos representantes desta classe de produtos naturais. O padrão de oxigenação típico do núcleo benzofenônico e a ciclização intramolecular para formar o anel biciclo[3.3.1]noneno são apreciados na suposta via biossintética de uma benzofenona tetraprenilada, epiclusianona, exposta no Esquema 1 (Santos et al., 1999). Vários derivados de benzofenonas preniladas com propriedades anti-HIV, denominadas de gutiferonas, foram isoladas anteriormente de extratos de plantas da família Guttiferae, principalmente de três gêneros distintos (*Garcinia, Clusia* e *Symphonia*). Uma destas benzofenonas poliisopreniladas, gutiferona A, foi inicialmente isolada de *Symphonia globulifera* como um composto ativo contra HIV (Gustafson et al., 1992), sendo posteriormente isolada de *Garcinia intermedia* (Abe et al., 2004). O amplo espectro de potenciais atividades biológicas de gutiferonas

inclui a inibição de efeitos deletérios às células hepáticas decorrentes da infecção *in vitro* causada por HIV (Gustafson et al., 1992); seqüestrador de radicais livres; inibição da expressão de iNOS e COX-2 no carcinoma de cólon intestinal; indução da apoptose e propriedades antiulcerosas, antioxidantes e tripanocidas (Abe et al., 2004; Pan et al., 2001; Tanaka et al., 2000; Yamaguchi et al., 2000a, b).

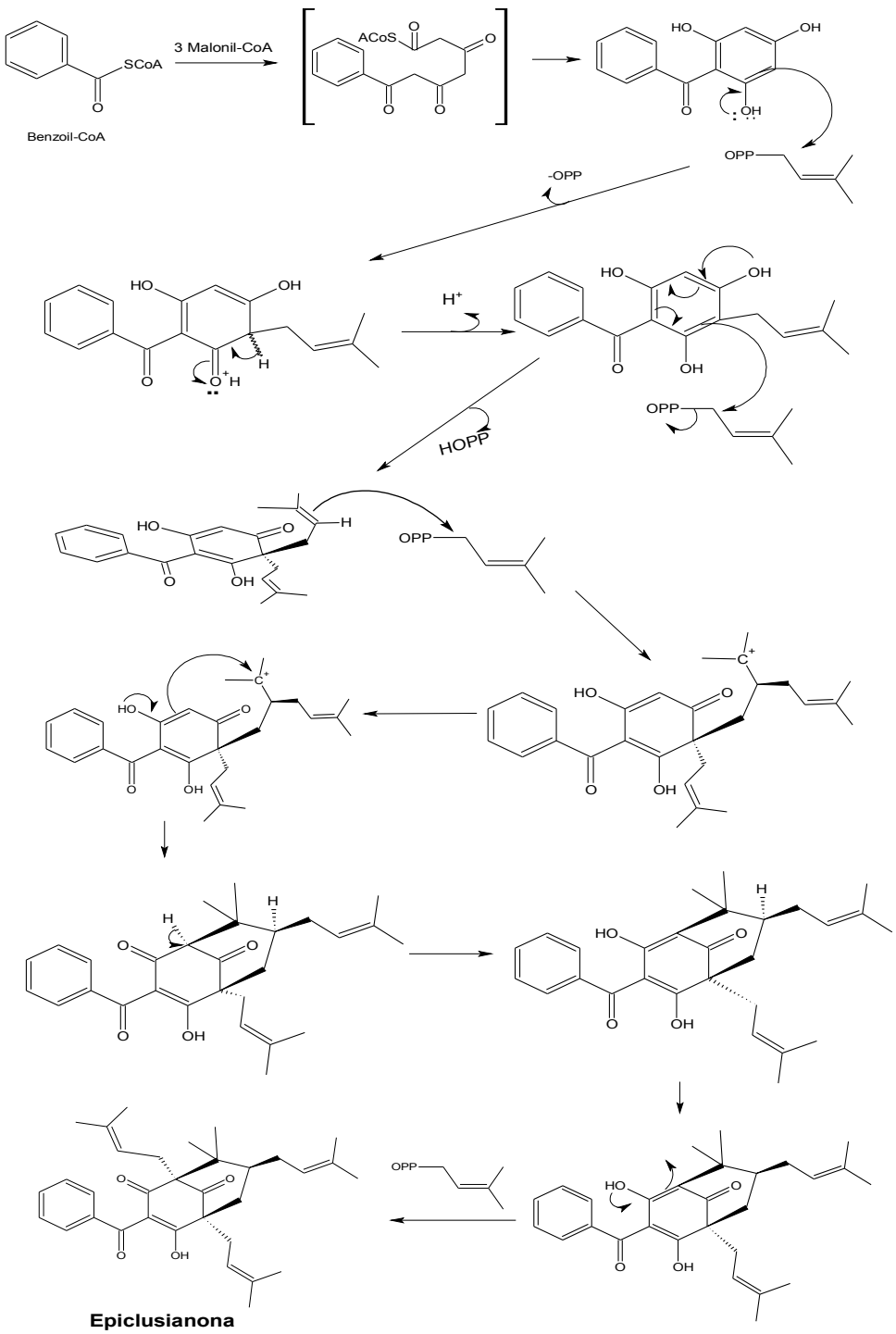

Esquema 1. Provável via biossintética de epiclusianona (Santos et al., 1999).

1.2 GÊNERO RHEEDIA

Garcinia ou Rheedia é o gênero mais numeroso da família *Guttiferae* com aproximadamente 400 espécies amplamente distribuídas na Ásia tropical, África, Polinésia e Brasil (Waterman, 1986). Este gênero é comumente usado na medicina popular brasileira e também é conhecido por ser rico em derivados fenólicos oxigenados e prenilados (Bennett e Lee, 1989), incluindo as benzofenonas isopreniladas (Rubio et al., 2001). Algumas destas apresentam várias atividades biológicas, como propriedades antifúngicas (Sordat-Diserens et al., 1991), antiinflamatórias (Khanum et al., 2004), antitumorais (Diaz-Carbalho et al., 2003) e antioxidantes (Merza et al., 2004), como também atuam na inibição da hiperlipidemia (Yamaguchi e Ariga, 2000).

1.3 BENZOFENONAS PRENILADAS

Em estudo anterior, foi isolada uma nova benzofenona tetraprenilada distinta das gutiferonas, epiclusianona, dos frutos de um espécime de *Rheedia gardneriana*, coletados em Viçosa, Minas Gerais, Brasil (Santos et al., 1999). Vários ensaios biológicos têm sido realizados com epiclusianona, mostrando atividades *in vitro* contra as formas tripomastigotas de *Trypanosoma cruzi* e contra *Artemia salina* (Alves et al., 1999). Também foi descrito efeito vasodilatador endotélio-dependente a baixas concentrações de epiclusianona em anéis aórticos de ratos (Cruz et al., 2006).

Apesar de toda relevância farmacológica desta classe de benzofenonas presente nas espécies de Guttiferae, especialmente no gênero Rheedia, existem dúvidas relativas a dados publicados tanto para epiclusianona e seu isômero clusianona, quanto para elucidação estrutural de gutiferona A. Quando isolada pela primeira vez, de raízes de *Clusia congestiflora* (McCandlish et al., 1976), a clusianona foi inambiguamente identificada por análises de difração de raios X (DRX) de monocristal, sendo estabelecida a orientação equatorial do grupo 3-metil-2-butenil em C-7. Já a molécula isolada dos frutos de *Rheedia gardnerina,* provenientes de Viçosa (Santos et al., 1999), analisada por DRX de monocristal e

Ressonância Magnética Nuclear (RMN), apresentou orientação axial do grupo 3-metil-2-butenil em C-7, sendo então caracterizada como epiclusianona. No entretempo desde a identificação inicial da clusianona em 1976 até o estabelecimento da variação estereoquímica do grupo prenila em C-7 com a identificação de epiclusianona em 1999, demais estudos foram conduzidos com partes de plantas pertencentes à família Guttiferae, nos quais foram possíveis identificações de clusianona baseadas apenas em dados espectroscópicos obtidos por RMN (Delle Monache et al., 1991; De Oliveira et al., 1996). Estes estudos contradisseram os dados de RMN para clusianona, sugerindo que estes compostos poderiam vir a ser epiclusianona, o que foi mais tarde confirmado por Santos et al. (1999) usando DRX. Destas observações advém a necessidade de investigações minuciosas destas benzofenonas poliprenildas, especialmente acerca da configuração estereoquímica em carbonos assimétricos, sendo indispensáveis análises de DRX para a confirmação estrutural de tais compostos. Além disso, estudos realizados para a gutiferona A mostraram que, dependendo do solvente utilizado nas mensurações de espectros de RMN, a duplicidade de sinais pode ser vista, inferindo a presença de dois constituintes (Gustafson et al., 1992). Este comportamento de gutiferona A deve-se ao equilíbrio ceto-enólico em solução. Contudo, a influência de parâmetros analíticos neste equilíbrio é pouco conhecida. Se não bastasse, outras determinações não foram realizadas até o presente momento, como a confirmação da estereoquímica de gutiferona A via análise de difração de raios X e a detecção do tautômero mais estável no estado sólido cristalino, bem como a concordância desta forma tautomérica com aquelas presentes em soluções.

1.4 A CRISTALOGRAFIA COMO FERRAMENTA PARA DETERMINAÇÃO DA ESTRUTURA QUÍMICA DE PEQUENAS MOLÉCULAS

1.4.1 Cristalografia: uma breve abordagem

A difração de raios X é um método de análise muito utilizado na caracterização de pequenas moléculas, uma vez que a partir da estrutura cristalina toda a informação espacial dos átomos que a constitui pode ser obtida com alta

precisão. O termo estrutura cristalina refere-se à distribuição dos átomos no interior de um cristal, um sólido com ordenamento dos constituintes atômicos a longo alcance. Um cristal consiste de celas unitárias, as quais são paralelepípedos definidos pelo empacotamento periódico das moléculas, abarrotadas ordenadamente e idênticas no que se refere à forma, tamanho e orientação. A cela unitária é definida por três vetores convergentes, e desta forma, por três ângulos formados entre estes vetores. A unidade fundamental desta distribuição é repetida regularmente, em três dimensões, no interior do cristal. Generalizando, toda e qualquer estrutura cristalina será definida por um grupo espacial, no qual estão implícitos o sistema cristalino, a classe do cristal e os elementos de simetria, pelas dimensões da cela unitária e pelas coordenadas atômicas. Por sua vez, os vetores que delimitam a cela unitária e os ângulos correspondentes originam os sete sistemas cristalinos, conforme os comprimentos axiais e valores dos ângulos interaxiais. Os sete sistemas cristalinos são: Triclínico, Monoclínico, Ortorrômbico, Tetragonal, Hexagonal, Romboédrico (trigonal) e Cúbico (Hahn, 2005). As faces das celas unitárias são codificadas pelas letras maiúsculas A, B e C, as quais contêm os eixos b e c, c e a, ou a e b, respectivamente. Os ângulos entre os respectivos pares de eixos anteriormente citados são convencionalmente conhecidos como α, β e γ.

A rede cristalina é definida por um arranjo regular de pontos no espaço e é por definição uma abstração puramente matemática, sendo que para elementos ou estruturas cristalinas iônicas cada ponto na rede pode ser um único átomo, enquanto que em moléculas orgânicas um grupo de átomos está freqüentemente anexado a um ponto da rede ou situado em um paralelepípedo primário. Existem cinco orientações básicas para os pontos de rede em uma cela unitária, as quais recebem os símbolos P (cela primitiva, com os pontos da rede localizados nos vértices da cela), C (base centrada, com os pontos centrados nas faces C e nos vértices das celas unitárias), F (face centrada, com os pontos da rede situados em todas as faces e nos vértices das celas unitárias), I (corpo centrado, com os pontos da rede situados no centro e nos vértices das celas unitárias) e R (cela romboédrica, a qual pode ser definida por uma cela primitiva hexagonal) (Hahn, 2005). Totalizando, 14 redes

espaciais, denominadas redes de Bravais, podem ser descritas através da combinação dos sete sistemas cristalinos com as condições de centragem de cela matematicamente possíveis para cada um dos sete sistemas cristalinos. A simetria que relaciona os átomos e a célula unitária deve ainda considerar os vários elementos de simetria pontuais (rotações, reflexões, inversões e roto-reflexões) e translacionais (roto-translações ou eixos parafusos e planos de deslizamento; Figura 1) a fim de somar os 230 grupos espaciais que descrevem a distribuição dos átomos ou moléculas dentro de uma cela unitária (Azároff, 1968).

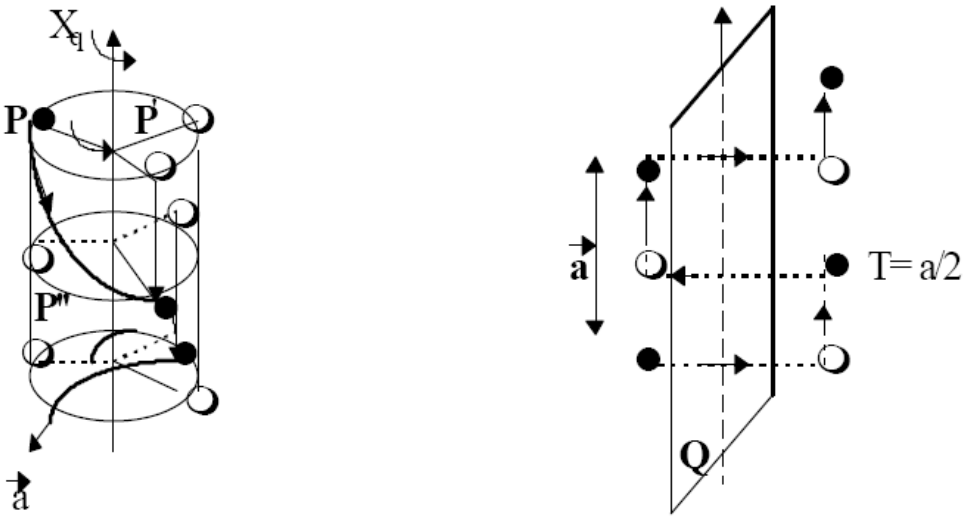

Figura 1. Uma visão esquemática de um eixo parafuso (à esquerda) e de um plano de deslizamento (à direita).

1.4.2 Difração de raios X aplicada à determinação da estrutura cristalina

Após esta breve descrição de conceitos básicos de cristalografia, uma introdução referente à difração de raios X será apresentada, enfocando a aplicação desta técnica na determinação estrutural de pequenas moléculas.

Primeiramente, raios X são ondas eletromagnéticas de λ entre 10^{-10}-10^{-8} m. raios X utilizados em difração apresentam λ na faixa de 0.5 a 2.5 Å. A difração pode ser definida como um fenômeno de espalhamento de radiação eletromagnética por um arranjo periódico de centros espalhadores. Como premissa básica, os centros espalhadores e a radiação a ser espalhada devem possuir grandezas espaciais de magnitude similar. Quando difratados, os raios X informam os tipos de átomos que

constituem o centro espalhador em função da densidade eletrônica dos mesmos, arranjo atômico (coordenadas dos átomos na cela unitária) e parâmetros cristalinos.

Um importante conceito para a interpretação da DRX por cristais é que três pontos não colineares da rede cristalina constituem um plano cristalográfico, o qual é referenciado por índices de Miller (Giacovazzo et al., 1994), uma simbologia representada por (h k l), onde h, k e l assumem números inteiros positivos ou negativos (barra acima do número), que leva em consideração as interseções do plano com os vetores da cela unitária (Figura 2). Vale ressaltar que, devido à simetria dos sistemas cristalinos, vários planos da rede não paralelos entre si apresentam equivalência cristalográfica e, assim, os números inteiros relativos aos índices de Miller h k l são dados entre chaves {} para este conjunto de planos coincidentes (dependentes por simetria). Para que exista interferência construtiva, e, conseqüentemente, o fenômeno da difração ocorra, há necessidade do feixe de raios X incidente formar um ângulo adequado em relação aos planos de rede acima contextualizados, precisamente, quando o ângulo de incidência e o ângulo de difração, θ, satisfazem à condição de Bragg, $n\lambda = 2d\text{sen}\theta$, onde λ é o comprimento de onda da radiação, d é o espaçamento interplanar associado aos índices de Miller e n é a ordem de difração, a qual deve ser obrigatoriamente um número inteiro. Somente ocorrerá interferência construtiva e o fenômeno da difração será percebido, quando a diferença de caminho entre duas ondas refletidas por planos de difração for igual a $n\lambda$.

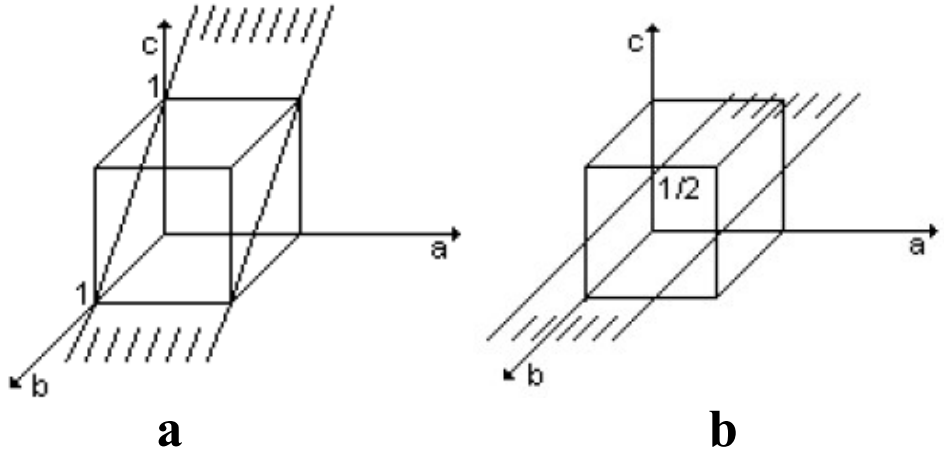

a **b**

Figura 2. Ilustração de dois planos cristalográficos atravessando uma cela unitária cúbica. **a:** plano (011); **b:** plano (002).

O espalhamento causado pelos elétrons na célula unitária resulta em uma função de interferência. Considerando que um elétron isolado espalha raios X com intensidade qualquer, um átomo de Z elétrons espalharia raios X com intensidade igual ao produto entre Z e a intensidade de um único elétron isolado. Entretanto, devido às distâncias entre os átomos serem da ordem do comprimento de onda dos raios X, as ondas que os elétrons espalham interferem umas com as outras, de forma que só teremos uma dada intensidade correspondendo a todos os elétrons de um átomo na direção de incidência dos raios X. Para o espalhamento em outras direções temos interferência parcialmente destrutiva, assim, a amplitude total cai com o aumento do ângulo de espalhamento. Desta observação podemos retirar a seguinte informação: a amplitude total do feixe espalhado é a soma das contribuições de todos os elétrons, ou seja, é proporcional ao número atômico. Estes valores de espalhamento constituem na amplitude normalizada do número de elétrons envolvidos, em outras palavras, é a relação entre a amplitude espalhada por um átomo e a amplitude espalhada por um elétron isolado, sob condições idênticas. Basicamente, esta é a definição de fator de espalhamento atômico, o qual pode assumir como valor máximo Z (número atômico do átomo) na ocasião dos elétrons espalharem a radiação, em fase, na direção de incidência ($2\theta = 0$). Para os feixes espalhados na direção da incidência, os raios X estarão em fase e a amplitude é somada. Quando o ângulo de difração é diferente de zero, as trajetórias dos raios espalhados são diferentes e a diferença de fase resulta em interferência. Considerando uma molécula, a onda total espalhada por todos os átomos é dada pela soma vetorial das contribuições individuais de cada átomo.

Em prática, o fator de espalhamento atômico significa a tendência de um átomo para espalhar a radiação X, a um dado ângulo e certo λ. Assim, valores tabelados são encontrados para razões de $\text{sen}\theta/\lambda$, expressos como o quociente entre a amplitude da onda espalhada por um átomo sobre a amplitude da onda espalhada por um elétron. De maneira similar ao fator de espalhamento atômico, o fator de estrutura é um quociente de duas amplitudes: a amplitude da onda espalhada por todos os átomos da célula unitária e a amplitude da onda espalhada por um elétron isolado, onde a magnitude deste fator depende unicamente da disposição relativa de

todos os átomos na célula unitária e de seus respectivos fatores de espalhamento. Provem da equação do fator de estrutura a necessidade de calcular o somatório das contribuições relativas de todos os átomos na célula unitária. Este fator é um número complexo por expressar tanto a amplitude quanto a fase da onda.

Experimentalmente, quando um monocristal de um dado composto, obtido através de cristalização e/ou recristalização a partir de solventes comuns, é irradiado com raios X, de λ da ordem de 1,0 Å, ele se comporta como uma rede de difração tridimensional e produz um padrão de difração constituído de um arranjo tridimensional de intensidades difratadas. As intensidades destas reflexões estão intimamente relacionadas à densidade eletrônica dos átomos espalhadores, uma vez que o padrão de difração é a transformada de Fourier da densidade eletrônica da estrutura e, inversamente, a densidade eletrônica da estrutura é a transformada de Fourier do padrão de difração. Desta forma, através das intensidades e direções das reflexões difratadas é possível determinar a densidade eletrônica da estrutura, partindo de duas premissas fundamentais: 1) a intensidade difratada para um dado conjunto h k l é aproximadamente o quadrado do fator de estrutura para o respectivo conjunto de índices de Miller, possibilitando, então, o cálculo da amplitude dos fatores de estrutura (mas não a fase); 2) os fatores de estrutura são a transformada de Fourier da densidade eletrônica em dado volume (infinitesimal) da cela unitária e, portanto, a densidade eletrônica é a transformada de Fourier inversa dos fatores de estrutura. Uma vez conhecidos os fatores de estrutura, F(h k l), para todas as reflexões h k l, a densidade eletrônica, ρ(x y z), pode ser calculada para cada ponto x y z na cela unitária, viabilizando a construção de mapas de densidade eletrônica de uma molécula em um cristal. Quando um mapa de boa resolução é calculado, os pontos de máxima densidade eletrônica correspondem ao centro dos átomos e, consequentemente, às suas posições (Warren, 1959). O grande problema no cálculo desses mapas é a obtenção das fases relativas dos fatores de estrutura, que representam os ângulos de fase dos raios X difratados, sendo este o problema crítico no método, o qual é resolvido, por exemplo, através de modelos estatísticos e suposições químicas razoáveis. Neste caso, denominado Método Direto, a obtenção de informação das fases dos fatores de estrutura é conseguida diretamente das

amplitudes observadas, onde reflexões fortes correspondem a regiões com uma densidade eletrônica elevada, sendo, portanto, as mais importantes na determinação da informação de fase. Neste procedimento, os fatores de estrutura com altas amplitudes têm suas fases atribuídas, avaliando, em seguida, se o mapa da densidade eletrônica obtido apresenta algum sentido químico. Posteriormente, as fases das demais reflexões são determinadas, da mesma forma que as fases das reflexões fortes foram encontradas (Figura 3).

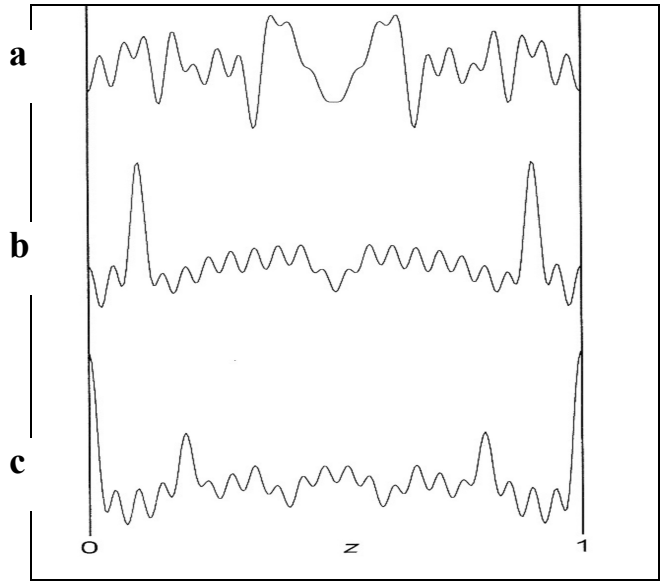

Figura 3. Densidade eletrônica em uma cela unitária contendo duas moléculas de ácido 3-bromo-octadecanóico, distribuída a partir das relações entre as fases das reflexões 00*l* mais intensas. **a**: fases escolhidas aleatoriamente, fornecendo um resultado sem sentido químico; **b**: as fases das reflexões (004) e (005) foram corretamente atribuídas, permitindo a determinação das fases de outras reflexões relacionadas. Neste caso, os dois máximos de densidade eletrônica correspondem aos átomos de bromo e os mínimos aos átomos de carbono; **c**: todas as fases positivamente atribuídas, gerando um mapa de densidade eletrônica sem significado cristalográfico.

Desde que a estrutura molecular inicial foi obtida, as posições atômicas (coordenadas fracionárias e fatores de vibração térmica) são refinadas utilizando o método de Mínimos Quadrados até se obter o melhor ajuste entre os dados de intensidade observados e os calculados de acordo com o modelo da estrutura preliminar. A cada reflexão é dado um peso *w* que representa a confiança na

importância dessa reflexão na somatória, geralmente, uma estimativa da precisão da medida da amplitude. O progresso do refinamento é monitorado usando os fatores residuais, os quais levam em consideração os fatores de estrutura calculados a partir da densidade eletrônica (ou informação de fase) dada pelos átomos obtidos na solução inicial. Por fim, a diferença entre os fatores de estrutura calculados e observados é minimizada usando o procedimento de mínimos quadrados de matriz completa, ajustando as posições e os fatores de temperatura dos átomos do modelo, sendo que estes últimos são refinados anisotropicamente através de seis parâmetros térmicos por átomo. Estes parâmetros térmicos, quando modelados por um tensor simétrico, chamado elipsóide térmico, melhora a descrição da densidade eletrônica e fornecem resultados importantes para uma comparação detalhada de distâncias interatômicas e ângulos, apesar de incrementar o tempo computacional de cada ciclo de refinamento.

1.5 ENZIMAS PROTEOLÍTICAS

Uma abordagem estrutural, funcional e fisiopatológica sobre as enzimas utilizadas nos ensaios descritos no subitem 4.1 é apresentada nesta seção, com intuito de expor, em um primeiro momento, características inerentes às proteases avaliadas essenciais para o estabelecimento e compreensão de relações entre as estruturas cristalograficamente determinadas de benzofenonas naturais e sintéticas e a atividade antiproteolítica desta classe de compostos.

1.5.1 Proteases

Proteases ou peptidases caracterizam uma larga família de enzimas conhecidas por catalisarem ligações peptídicas. Podem ser classificadas como endopeptidases e exopeptidases de acordo com o local onde clivam a cadeia peptídica. Estas enzimas podem ser classificadas em quatro grandes grupos ou famílias de acordo com os aminoácidos do sítio ativo envolvidos na catálise. Podem ser classificadas como serino, cisteíno, aspartato e metalo-proteases. As enzimas que apresentam características comuns como, por exemplo, estrutura primária

homóloga e aminoácidos importantes para o mecanismo de catálise, são agrupadas em famílias e clãs (Tabela 1).

Em termos numéricos, as serino-proteases foram mais extensamente investigadas. Este é considerado o grupo mais caracterizado entre todas as subdivisões de proteases (Otto e Schirmeister, 1997). Cisteíno-proteases, também conhecidas como tiol-proteases, já foram encontradas em vírus, bactérias, protozoários, plantas e mamíferos (Barret e Salvesen, 1986). Recentemente, cisteíno-proteases têm sido encontradas em fungos (Sharma et al., 1989).

TABELA 1 - Classificação de proteases de acordo com seu mecanismo de catálise.

	Protease representativa	Aminoácidos presentes no sítio catalítico
SERINO PROTEASE		
Clã SA	Tripsina, Quimotripsina	His, Asp, Ser
Clã SB	Subtilisina	Asp, His, Ser
Clã SC	Carboxipeptidase C	Ser, Asp, His
Clã SE	Carboxipeptidase de *Streptomyces*	Ser, Lys
Clã SF	Repressor Lexa	Ser, Lys
Clã SH	Assemblina de Citomegalovírus	His, Ser, His
CISTEÍNO PROTEASE		
Clã CA	Papaína	Cys, His, Asn
Clã CB	Endopeptidases virais quimotripsina-like	His, Cys, Glu
Clã CC	Endopeptidases virais papaína-like	Cys, His
Clã CD	Caspase	His, Cys
Clã CE	Endopeptidase de Adenovírus	His, Glu, Cys
ASPARTIL-PROTEASE		
Clã AA	Pepsina	Asp, Asp
Clà AB	Endopeptidase de Nodavírus	Asp, Asp
METALO-PROTEASE		
Clã MA	Termolisina	Glu, Asp, His/Zn^{2+}
Clã MB	Astacina	His, His, His(/Asp)/ Zn^{2+}
Clã MC	Metalocarboxipeptidase	His, Glu, His/ Zn^{2+}
Clà MD	Zinco D-Ala-D-Ala peptidase	His, Asp, His/ Zn^{2+}
Clã ME	Pitrilisina	His, His, Glu/ Zn^{2+}

Clã MF	Leucil aminopeptidase	Asp, Asp, Glu, Zn^{2+}, Asp, Lys, Asp, Zn^{2+}
Clã MG	Metionil aminopeptidase	Asp, His, Glu, Co^{2+}, Asp, Asp, Glu, Co^{2+}

1.5.2 Cisteíno-proteases: Papaína

Entre as cisteíno-proteases, a mais investigada é a papaína (EC 3.4.22.2), oriunda do látex de *Carica papaya*. Papaína é um polipeptídeo monomérico com peso molecular de 23406 Da, consiste de uma cadeia de 212 resíduos de aminoácidos com três ligações dissulfeto (Cys22-Cys63, Cys56-Cys95, Cys153-Cys200). A seqüência e a estrutura tridimensional são conhecidas (Kamphuis et al., 1984; Lowe, 1976), assim como a estrutura do complexo papaína-E-64, um inibidor irreversível desta enzima, foi determinada por análise de difração de raios X (Varughese et al., 1989). Papaína é particularmente eficaz na clivagem de peptídeos contendo resíduos de Arg e Lys (P1), mas o subsítio que reconhece estes resíduos provenientes do substrato peptídico tem uma especificidade muito menos definida que S2, o qual prefere resíduos hidrofóbicos como Phe. O subsítio S2 da papaína é uma bolsa hidrofóbica formada por resíduos dos aminoácidos Trp69, Tyr67, Phe207, Pro68, Ala160, Val133 e Val157 (Brocklehurst et al., 1987). Papaína é isolada numa forma inativa e a sua ativação é possível por reações das pontes dissulfeto intramoleculares com tiol-reagentes ou agentes redutores. Papaína é formada a partir de um zimogênio clássico (pró-papaina) (Cohen et al., 1986).

1.5.3 Cisteíno-proteases: Catepsina B

Hoje, mais de 450 proteases já têm sua seqüência de aminoácidos determinada. Catepsinas são peptidases lisossomais e estão envolvidas em diversas patologias. Entre todas as cisteíno-proteases lisossomais, a Catepsina B (EC 3.4.22.1) é a mais intensamente estudada. Esta enzima tem sido isolada de vários tecidos de mamíferos e de diferentes espécies, apresentando alta similaridade estrutural quando a seqüência de aminoácidos de espécies distintas é considerada

(Baricos et al., 1988). A estrutura tridimensional da catepsina B foi determinada pela primeira vez em 1991 (Musil et al., 1991). Catepsina B é uma glicoproteína apresentando um resíduo de carboidrato espécie-específico ligado, geralmente, ao aminoácido Asn (Asn 110/113) (Taniguchi et al., 1985). O peso molecular da glicoproteína é aproximadamente 29 kDa, e 27 kDa é o peso molecular da fração peptídica. Esta cisteíno-protease também é formada a partir de uma pró-enzima, como no caso de papaína. Um peptídeo sintético, correspondente à pró-região da catepsina B, foi sintetizado como um potente inibidor de Catepsina B, e o seu mecanismo de inibição está baseado no bloqueio do sítio ativo enzimático (Cygler et al., 1996). Catepsina B raramente tem sido detectada no compartimento extracelular de tecidos não-patológicos, devido a sua baixa estabilidade em pH neutro a alcalino (Kirschke et al., 1987). Contudo, isoformas estáveis em meios alcalinos foram encontradas no compartimento extracelular de tecidos tumorais, na sua maioria, apresentando peso molecular maior que os respectivos valores das isoformas intracelulares (Brocklehurst et al., 1987; Kirschke et al., 1987). A comparação das seqüências de catepsina B, catepsina H, papaína e actinidina demonstra que as estruturas terciárias destas enzimas são muito similares (Dufour, 1988). Aproximadamente 166 resíduos de aminoácidos da catepsina B são topologicamente equivalentes àqueles da papaína, mas, mudanças na extensa estrutura resultantes de inserções em uma região da cadeia polipeptídica (entre os resíduos de número 106 e124) levam à oclusão de alças. Estas alterações acarretam diferentes especificidades. Catepsina B pode apresentar tanto atividade de exopeptidase quanto de endopeptidase (Mort e Buttle, 1997). Abaixo de pH 5,5, ela apresenta atividade essencialmente de uma exopeptidase, com atividade proteolítica lisossomal. Acima de pH 5,5, começa ocorrer uma mistura de formas capazes de atuar como endo e exopeptidase e, por volta de pH 7,4, Catepsina B exibe sua máxima atividade como endopeptidase. Em invasões tumorais e metástase, Catepsina B foi encontrada fora do compartimento lisossomal com atividade de endopeptidase, desempenhando um papel importante na degradação de matriz extracelular e membrana basal (Polgar e Csoma, 1987). Entretanto, o aumento da expressão, atividade e secreção da Catepsina B tem sido observado em mais de um

tipo de tumor, tais como no carcinoma de pulmão, de estômago, de mama e de próstata (Koblonski et al., 2000).

1.5.4 Serino-proteases: Catepsina G

A Catepsina G humana é uma das principais enzimas proteolíticas encontradas nos grânulos azurófilos de leucócitos polimorfornucleares (neutrófilos) (Baggiolini et al., 1978) e é classificada como uma serino-protease (EC 3.4.21.20). Encontrada em mastócitos e monócitos (Sênior e Campbell, 1984), durante reações inflamatórias, esta enzima está envolvida na degradação de organismos estranhos ou tecidos mortos dentro do fagolisossoma (Watorek et al., 1988). Catepsina G é liberada no espaço extracelular, por extravasamento e/ou morte celular, onde é controlada por inibidores plasmáticos tais como α_1-antiquimotripsina e α_1-inibidor de protease. Um descontrole na regulação da atividade desta protease, ou em uma inflamação crônica, pode resultar em uma digestão desordenada de muitas proteínas e, também, da matriz extracelular (Bieth, 1986). As proteases do neutrófilos como a Catepsina G e elastase podem contribuir para o desenvolvimento de doenças do tecido conectivo como enfisema, artrite reumatóide e periodontite. Recentes estudos sugerem funções alternativas para Catepsina G em vários processos celulares, como a ativação de plaquetas (LaRosa et al., 1994), quimiotaxia de neutrófilos e monócitos (Chertov et al., 1997) e aumento de "natural killers" (Yamazaki e Aoki, 1998). Catepsina G também possui uma potente atividade antibacteriana que é independente da sua atividade de serino-protease (Shafer et al., 1991). A atividade proteolítica da Catepsina G tem sido estudada utilizando uma variedade de substratos peptídicos e proteínas. Esta enzima está envolvida na proteólise de elastina, colágeno tipo I e II, proteoglicanos cartilaginosos, fibronectina, laminina e imunoglobulinas G e M (Bieth, 1986). Catepsina G é também capaz de interagir com uma proteína do HIV (Avril et al., 1995), assim como está envolvida no processo de ativação proteolítica de interleucina-8 (Padrines et al., 1994), na ativação de C3 do sistema complemento (Maison et al., 1991) e fator V (Allen e Tracy, 1995). A investigação da especificidade de Catepsina G por substratos já foi

conduzida utilizando cadeias de insulina (Levy e Feinstein, 1979), substratos peptídicos com 4-nitroanilida (Tanaka et al., 1985) e peptídeos derivados de tio-éster (Harper et al., 1981), a qual tem mostrado a especificidade tanto "quimotrypsin-like" quanto "trypsin-like". Entretanto, sua atividade sobre todos os substratos sintéticos testados até agora é muito menor quando comparada com a atividade de serino-proteases homólogas sobre estes peptídeos.

1.5.5 Serino-proteases: Tripsina

A tripsina (E.C. 3.4.21.4) é uma das serino-proteases mais estudadas até o momento. Esta enzima tem especificidade para ligações peptídicas contendo resíduos de cadeia lateral carregada positivamente, tais como Arg e Lys, na posição P1 do substrato. No caso da tripsina, o mecanismo de hidrólise peptídica baseia-se em um ataque nucleofílico às ligações peptídicas por um resíduo de serina. A propriedade nucleofílica do grupo hidroxila da serina é incrementada pela presença de uma histidina, mantida num "estado receptor de prótons" por um aspartato. As cadeias laterais dos resíduos de serina, histidina e aspartato formam a tríade catalítica, comum nas serino-proteases (Beynon e Bond, 1989).

2 REFERÊNCIAS

Abe, F.; Nagafuji, S.; Okabe, H.; Akahane, H.; Muñiz, E.E.; Reyes, M.H.; Chilpa, R.R. **Biol. Pharm. Bull**. 27: 141-143, 2004.

Allen, D.H.; Tracy, P.B. **J. Biol. Chem**. 270: 1408-1415, 1995.

Alves, T.M.; Alves, R.; Romanha A.J.; Zani, C.L.; Dos Santos, M.H.; Nagem, T.J. **J. Nat. Prod.** 62: 369-711, 1999.

Avril, L.E.; di Martino-Ferrer, M.; Brillard-Bourdet, M.; Gauthier, F. **FEBS Lett**. 367: 251-256, 1995.

Azároff, V.L. **Elements of X-ray Crystallography**. McGraw-Hill Book Company, New York, 1968.

Baggiolini, M.; Bretz, U.; Dewald, B.; Feigenson, M.E. **Agents Actions** 8: 3-10, 1978.

Baricos, W.; Zhou, Y.; Mason, R.; Barrett, A. **Biochem. J.** 252: 301-304, 1988.

Barrett, A.; Salvesen, G. **Proteinase Inhibitors**. Elsevier, Amsterdam, 1986.

Bennett, G.; Lee, H.H. **Phytochemistry** 28: 967-998, 1989.

Beynon, R.J.; Bond, **J.S. Proteolytic enzymes: a practical approach**. Liverpool, Oxford University, 1989.

Bieth, J.G. Em: **Biology of the Extracellular Matrix;** Mecham, R.P. (Ed.). vol. 1, Academic Press, New York, 1986, pp. 217-320.

Brocklehurst, K.; Willenbrock, F.; Salih, E. Em: **New Comprehensive Biochemistry;** Neuberger, A.; Brocklehurst, K. (Eds.). Elsevier, Amsterdam, 1987, pp. 39-158.

Chertov, O.; Ueda, H.; Xu, L.L.; Tani, K.; Murphy, W.J.; Wang, J.M.; Howard, O.M.; Sayers, T.J.; Oppenheim, J.J. **J. Exp. Med.** 186: 739-747, 1997.

Cohen, L.; Coghlan, V.; Dihel, L. **Gene** 48: 219-227, 1986.

Cruz, A.J.; Lemos, V.S.; Dos Santos, M.H.; Nagem, T.J.; Cortes, S.F. **Phytomedicine** 13: 442-445, 2006.

Cygler, M.; Sivaraman, J.; Grochulski, P.; Coulombe, R. **Structure** 4: 405-416, 1996.

De Oliveira, C.M.A.; Porto, A.M.; Bittrich, V.; Vencato, I.; Marsaioli, A.J. **Tetrahedron Lett.** 37: 6427–6430, 1996.

Delle Monache, F.; Delle Monache, G.; Gacs-Baits, E. **Phytochemistry** 30: 2003–2005, 1991.

Díaz-Carballo, D.; Seeber, S.; Strumberg, D.; Hilger, R.A. **Int. J. Clin. Pharm. Th.** 41: 622-623, 2003.

Dufour, E. **Biochimie** 70: 1335-1342, 1988.

Giacovazzo, C.; Monaco, H.L.; Scordari, F. **Fundamentals of Crystallography.** Oxford University Press, New York, 1994.

Gustafson, K.R.; Blunt, J.W.; Munro, H.G.M.; Fuller, R.W.; McKee, C.T.; Cardellina, J.H.; McMahon, J.B.; Cragg, G.M.; Boyd, M.R. **Tetrahedron** 48: 10093–10102, 1992.

Hahn, T. (Ed.) **International Tables for Crystallography**. 5 ed., vol. 1, Springer, Dordrecht (The Netherlands), 2005.

Harper, J.W.; Ramirez, G.; Powers, J.C. **Anal. Biochem**. 118: 382-387, 1981.

Kamphuis, I.G.; Kalk, K.H.; Swarte, M.B.; Drenth, J. **J. Mol. Biol.** 179: 233-256, 1984.

Khanum, S.A.; Shashikanth, S.; Deepak, A.V. **Bioorg. Chem.** 32: 211-222, 2004.

Kirschke, H.; Barret, A. Em: **Lysosomes: Their Roles in Protein Breakdown**; Glaumann, B. (Ed.). Academic Press, London, 1987, pp. 193-238.

Koblonski, J.E.; Ahram, B.F.; Sloane, B.F. **Clin. Chim. Acta** 291: 113-135, 2000.

Lara, R.J. **Fundamentos de Cristalografia Fisica**. The General Secretary of the Organization of American States, Washington, 1986.

LaRosa, C.A.; Rohrer, M.J.; Benoit, S.E.; Rodino, L.J.; Barnard, M.R.; Michelson, A.D. **J. Vasc. Surg.** 19: 306-318, 1994.

Levy, H.; Feinstein, G. **Biochim. Biophys. Acta**. 567: 35-42, 1979.

Lowe, G. **Tetrahedron** 32: 291-302, 1976.

Maison, C.M.; Villiers, C.L.; Colomb, M.G. **J. Immunol.** 147: 921-926, 1991.

McCandlish, L.E.; Hanson, J.C.; Stout, G.H. **Acta Crystallogr. Sect. B** 32: 1793-1801, 1976.

Merza, J.; Aumond, M.C.; Rondeau, D.; Dumontet, V.; Le Ray, A.M.; Séraphin, D.; Richomme, P. **Phytochemistry** 65: 2915–2920, 2004.

Mort, J.S.; Buttle, D.J. **Int. J. Biochem. Cell Biol.** 29: 715-720, 1997.

Musil, D.; Zucic, D.; Turk, D.; Engh, R.; Mayr, I.; Huber, R.; Popovic, T.; Turk, V.; Towatari, T.; Katunuma, N.; Bode, W. **EMBO J.** 10: 2321-2330, 1991.

Otto, H.; Schirmeister, T. **Chem. Rev.** 97: 133-171, 1997.

Padrines, M.; Wolf, M.; Walz, A.; Baggiolini, M. **FEBS Lett.** 352: 231-235, 1994.

Pan, M.H.; Chang, W.L.; Lin-Shiau, S.Y.; Ho, C.T.; Lin, J.K. **J. Agric. Food Chem.** 49: 1464–1474, 2001.

Polgar, L.; Csoma, C. **J. Biol. Chem.** 262: 14448-14453, 1987.

Rubio, O.C.; Padron, A.; Castro, H.V.; Pizza, C.; Rastrelli, L. **J. Nat. Prod.** 64: 973-975, 2001.

Santos, M.H.; Nagem, T.J.; Oliveira, T.T.; Braz-Filho, R. **Quím. Nova** 22: 654-660, 1999.

Senior, R.M.; Campbell, E.J. **J. Immunol.** 132: 2547-2551, 1984.

Shafer, W.M.; Pohl, J.; Onunka, V.C.; Bangalore, N.; Travis, J. **J. Biol. Chem.** 266: 112-116, 1991.

Sharma, A.; Padwal-Desai, S.; Ninjoor, V. **Biochem. Biophys. Res. Commun**. 159: 464-471, 1989.

Sordat-Diserens, I.; Rogers, B.S.C.; Hostettmann, K. **Phytochemistry** 31: 313-316, 1991.

Tanaka, T.; Kohno, H.; Shimada, R.; Kagami, S.; Yamaguchi, F.; Kataoka, S.; Ariga, T.; Murakami, A.; Koshimizu, K.; Ohigashi, H. **Carcinogenesis** 21: 1183–1189, 2000.

Tanaka, T.; Minematsu, Y.; Reilly, C.F.; Travis, J.; Powers, J.C. **Biochemistry** 24: 2040-2047, 1985.

Taniguchi, T.; Mizuochi, T.; Towatari, T.; Katunuma, N.; Kobata, A. **J. Biochem.** 97: 973-976, 1985.

Varughese, K.; Ahmed, F.; Carey, P.; Hasnain, S.; Huber, C.; Storer, A. **Biochemistry** 28: 1330-1332, 1989.

Warren, E.B. **X ray Diffraction**. Addison-Wesley Pub.Company, London, 1959.

Waterman, P.G. **Trends Ecol. Evol.** 1: 110-111,1986.

Watorek, W.; Farley, D.; Salvesen, G.; Travis, J. **Adv. Exp. Med. Biol.** 240: 23-31, 1988.

Williams, R.B.; Hoch, J.; Glass, T.E.; Evans, R.; Miller, J.S.; Wisse, J.H.; Kingston, D.G.I. **Planta Med.** 69: 864–866, 2003.

Yamaguchi, F.; Ariga, T.; Yoshimura, Y.; Nakazawa, H. **J. Agric. Food Chem.** 48: 180–185, 2000a.

Yamaguchi, F.; Saito, M.; Ariga, T.; Yoshimura, Y.; Nakazawa, H. **J. Agric. Food Chem.** 48: 2320–2325, 2000b.

Yamaguchi, N.; Ariga, T. **Benzophenone derivatives from Garcinia plants as lipase inhibitor, anti-obesity agents, and hypolipidemics.** Número da Patente JP2000044468, 2000.

Yamazaki, T.; Aoki, Y. **Immunology** 93: 115-121, 1998.

3 PARTE 1: ELUCIDAÇÃO ESTRUTURAL DE GUTIFERONA A E GARCINIAFENONA

3.1 "NATURAL POLYPRENYLATED BENZOPHENONES: KETO-ENOL TAUTOMERISM AND STEREOCHEMISTRY"

MARTINS, F. T., CRUZ JUNIOR, J. W., DEROGIS, P. B. M. C., SANTOS, M. H., VELOSO, M. P., ELLENA, J., DORIGUETTO, A. C. Natural polyprenylated benzophenones: keto-enol tautomerism and stereochemistry. **Journal of the Brazilian Chemical Society**. 18(8): 1515-1523, 2007.

3.2 "GARCINIAPHENONE, A NOVEL NATURAL POLYPRENYLATED BENZOPHENONE FROM GARCINIA BRASILIENSIS"

MARTINS, F. T., CAMPS, I., DORIGUETTO, A. C., SANTOS, M. H., ELLENA, J., BARBOSA, L. C. A. Garciniaphenone, a novel natural polyprenylated benzophenone from *Garcinia brasiliensis*. **Journal of Molecular Structure**. *submitted*, 2007.

Garciniaphenone, a novel natural polyprenylated benzophenone from *Garcinia brasiliensis*

Felipe T. Martins,* I. Camps, Antônio C. Doriguetto and Marcelo H. dos Santos

Department of Exact Science, Federal University of Alfenas -37130-000, Alfenas - MG, Brazil

Javier A. Ellena

Institute of Physics of São Carlos, State University of São Paulo. - CP 369, 13560-970, São Carlos - SP, Brazil

Luiz C. A. Barbosa

Chemistry Department, Federal University of Viçosa -, 36571- 000, Viçosa – MG, Brazil (lcab@ufv.br)

∗ Corresponding to: Felipe T. Martins, Department of Exact Science, Federal University of Alfenas - UNIFAL-MG, Rua Gabriel Monteiro da Silva, 714, Alfenas - MG, 37130-000, Brazil (phone: (+55) 35 3299-1261; fax: (+55) 35 3299-1261). E-mail: felipetmartins@yahoo.com.br

Abstract

Garciniaphenone (3-benzoyl-4-hydroxy-6,6-dimethyl-1,7-bis(3-methyl-2-butenyl)bicycle[3.3.1]non-3-en-2,9-dione), is a new natural substance isolated from the hexanic extract of *Garcinia brasiliensis* fruits. Its crystal structure is reported in the present paper and some geometrical and stereochemical features were compared with those from analogous benzophenones. The title compound is the first one in the respective class of related polyprenylated benzophenones without a C5 prenyl substituent, which has influenced the molecular geometry. The tautomeric form of garciniaphenone in the solid state was readily established by residual electronic density map using difference Fourier analysis, although there is an entirely delocalized chelating six-membered system passing through the keto-enol moiety. In addition, we have rationalized the keto-enol tautomeric form of garciniaphenone based on stereochemistry of C7 atom, which was further strengthened by LUMO calculations. The intermolecular array in the network is achieved by non-classical intermolecular hydrogen bonds.

KEYWORDS: polyprenylated benzophenones, garciniaphenone, keto-enol tautomerism, X-ray diffraction analysis, LUMO calculation.

1. Introduction

Garcinia brasiliensis (Mart.) Planch. & Triana, (Syn. *Rheedia brasiliensis*), commonly known as "bacupari", is used in Brazilian traditional medicine for the treatment of urinary and tumor diseases [1]. *Garcinia* or *Rheedia* is the most numerous genus of the Guttiferae family and it is known to be rich in oxygenated and prenylated phenol derivatives [2], including xanthones [3], flavonoids [4], phenolic acids [5] and benzophenones [6]. Previous works have reported the presence of the biflavonoids volkensiflavone and fukugetina [7] and prenylated xanthones from the roots methanolic extracts of *G. brasiliensis* [2]. From the hexanic and ethanolic extracts from fruits and seeds of *G. brasiliensis* three prenylated benzophenones were isolated and purified by column chromatography and preparative thin layer chromatography. One of them, the title compound that we have named garciniaphenone (I), is a new natural substance reported for the first time in the present paper that is only found at the fruits. The two others compounds, epiclusianone (II) [8] and guttiferone A [9], have already been extracted from others species of the same family and can be obtained from *G. brasiliensis* seeds, whereas compound (II) is also the major secondary metabolite extracted from the fruits of this species. The crystal structures of compound (II) [8] and guttiferone A [10,11] have already been reported.

Polyprenylated benzophenones are biologically active compounds and are common metabolites from Guttiferae family. Some of them, including guttiferone A, were isolated from *Symphonia globulifera*, *Garcinia livingstonei*, *Garcinia ovalifolia* and *Clusia rosea* as HIV-inhibitory compounds [9]. Since then, these substances become target of extensive studies, mainly focused in the screening for further pharmacological properties on various biological systems. As a result, it is agreed that polyprenylated benzophenones also possess

free radical scavenging; iNOS and COX-2 expression inhibiting in colon carcinoma; apoptosis induction and antiulcer, antioxidant, trypanocidal [12-16], anti-inflammatory [17], and antitumoral properties [18]. Compound (II) presents vascular effects on the rat aorta [19] and anti-HIV activity [20].

We have studied the chemical structure of compound (I) by IR, MS, 2D-NMR, ^{1}H and ^{13}C NMR experiments [21]. The NMR spectra revealed the presence of a common behaviour in related benzophenones [9], a keto-enol equilibrium involving the 2,4-dione enolizable system. So, the ^{1}H NMR spectral data of compound (I) have pointed out a signal set corresponding to two hydroxyl groups from tautomers (Ia) and (Ib) at solution state, as it is depicted in Scheme 1. However, the interpretation of the NMR spectra was difficult. Through the crystal structure determination it is possible to identify the tautomer present in the solid phase, as well as to check if this structure is in agreement with that assigned by spectroscopic methods in solution. In this way, the X-ray diffraction analysis, reported here, has afforded the chemical form in the solid state of compound (I) and allowed us the unambiguous determination of its structure. Furthermore, *ab initio* calculations were carried out, mainly on the electronic properties as LUMO/HOMO surface location, in order to get insights on structural data of (I). For this purpose, XRD structures of (I), which has been determined for the first time in the present work, and clusianone, an analogous polyprenylated benzophenone [22], were used as starting point for comparative theoretical measurements.

Scheme 1

2. Experimental

2.1. Plant extraction and (I) isolation

Garcinia brasiliensis fruits were obtained from plants growing naturally in the *Campus* of Universidade Federal de Viçosa (UFV), Viçosa, Brazil, and later recognized by a botanist of UFV. The voucher specimen is deposited in Horto Botânico of UFV (register number VIC2604). Afterwards, the fruits were dried and powdered, which yield approximately 1 Kg that was macerated with 3L of n-hexane at room temperature by seven days. The solvent was then separated by filtration and removed under reduced pressure in a rotary evaporator 45°C. The overall procedure was repeated five times to yield a total of 80 g of *G. brasiliensis* fruit hexanic extract (**GBFHE**).

GBFHE was exhaustively chromatographed on silica gel (230-400 mesh) column (8 x 100cm) with mixtures of hexane:ethyl acetate (100:0 to 0:100 v/v) and ethyl acetate:ethanol (100:0 to 0:100 v/v) to give 50 fractions that were grouped according to their similarities by thin layer chromatography (TLC) analysis: **GBFHE -1** (fractions 1-6, 10g, a mixture of sesquiterpenes), **GBFHE-2** (fractions 7-20, 20g, resinous orange material) and **GBFHE-3** (fractions 21-50, 30g, a complex mixture). **GBFHE-2** was washed with acetone to produce two sub-fractions, differentiated as an insoluble portion (**GBFHE-2I**) containing 5g of a mixture of hydrocarbons, and another soluble one (**GBFHE-2S**). From **GBFHE-2S**, a yellow resinous material was separated after solvent evaporation. **GBFHE-2S** was rechromatographed on a silica gel column as it was previously described, giving 26 fractions that were pooled into 5 sub-groups: **GBFHE-2S(1-5)**. Through several recrystallizations of the **GBFHE-2S3** fraction (1.8 g) in methanol, 1.0 g of benzophenone (II) was isolated. **GBFHE-2S4** (8.0 g) was rechromatographed on a silica gel column to give 20 fractions, which were joined in 7 groups [**GBFHE-2S4(A-F)**]. Further 1.0 g of compound (II) was obtained from the sub-fractions **GBFHE-2S4A-B** by mean of recrystallization in methanol solution. Finally,

GBFHE-2S4C was recrystallized several times using the same solvent resulting in 0.65 g of compound (I).

2.2. Crystal purity and quantification of compounds (I) and (II)

Suitable crystals of benzophenones (I) and (II) were weighted (11 and 12 mg, respectively) and dissolved in methanol (10 mL), performing solutions at 1.1 and 1.2 g L^{-1} that were used to give the following dilutions in methanol:acetic acid 5% pH 3.84 (40:60 v/v, HPLC initial mobile phase): 40.0, 20.0, 10.0, 5.0 and 0.5 mg L^{-1}. From each previous dilution, it was injected in triplicate a volume of 20 μL (loop capacity) in the HPLC equipment (Shimadzu Corporation, Kyoto, Japan) equipped with two pumps (LC-10ATvp) and diode array detector (SPD-M10Avp) set at 254 nm. The analytical column was a C18 (150 mm×4.6 mm) with 5 μm particle size protected by a compatible guard column. The suitable gradient was achieved using methanol:acetic acid 5% pH 3.84 (40:60 v/v) to methanol 100% in 10 min with a solvent flow rate of 1.2 mL min^{-1} at 30 °C. The mobile phase solvents were filtered under vacuum using Millipore filter and degassed separately. ClassVP-LC10 software was used for data collection and acquisition. The HPLC analyses of compounds (I) and (II) at the five dilutions showed chromatograms with only a single strong signal referring to each benzophenone. The means ± standard deviation of the percent areas from all dilutions were 98.6±1.1 and 99.8±0.2%, respectively for compounds (I) and (II). So, the purity of the benzophenones has been considered suitable for an analytical standardization, and the diluted solutions were used as working standards to generate calibration curves. The quantification of compounds (I) and (II) in **GBFHE** extract was carried out by HPLC in triplicate under the same experimental chromatographic conditions used successfully with the working dilutions. The standard

curves were derived from linear regression analysis of the peak area ratios (analyte/internal standard) versus concentrations of the dilution, and the peak area ratios of compounds (I) and (II) at the **GBFHE** samples were interpolated in the generated calibration curves for quantification. Prior to **GBFHE** samples injection, 0.727, 0.689 and 0.750 g of this extract were separately treated with methanol (*ca.* 5 mL) at 40 °C during 10 min, quantitatively filtered using Whatman® 41 filter papers and the volumes were completed to 10 mL with methanol. From that, 25 μL was diluted to a final volume of 10 mL with methanol:acetic acid 5% pH 3.84 (40:60 v/v). To each final 10 mL of calibration standard solutions and **GBFHE** samples, an internal standard [(2,4-dihydroxyphenyl)(2-hydroxyphenyl)methanone] [23] at 10 g L^{-1} in methanol was added (final concentration of 100 mg L^{-1}).

2.3. X-Ray diffraction (XRD) experiment

Suitably shaped and sized clear single crystal of compound (I) was taken for the X-ray diffraction experiment. The intensity data were measured up to 56.24° in 2θ with the crystal at room temperature (293 K) and with graphite monochromated MoKα radiation (λ = 0.71073 Å), using the *Enraf-Nonius Kappa-CCD* diffractometer. The cell refinements were achieved using the softwares Collect [24] and Scalepack [25], and the final cell parameters were obtained on all 20638 reflections. Data integration and scaling were carried out using the software Denzo-SMN and Scalepack [25]. No absorption correction was required due to negligible absorption coefficient of 0.079 mm^{-1} for compound (I).

The structure was solved using the software SHELXS-97 [26] and refined using the software SHELXL-97 [27]. The C and O atoms were clearly solved and full-matrix least-squares refinement of these atoms with anisotropic thermal parameters was carried out.

The C-H hydrogen atoms were positioned stereochemically and were refined with fixed individual displacement parameters [U_{iso}(H) = 1.2U_{eq} (C_{sp}^2) or 1.5U_{eq} (C_{sp}^3)] using a riding model with aromatic C—H bond length of 0.93 Å, methyl C—H one of 0.96 Å, methylene C—H one of 0.97 Å and methine C—H one of 0.98 Å. The hydroxyl H atom was located by difference Fourier analysis and was set as isotropic. For that, the positional parameter of this H-atom was not constrained during refinements. Crystal, collection and structure refinement data are summarized in Table 1.

Table 1

Tables were generated by WinGX [28], and the softwares ORTEP-3 [29] and MERCURY [30] were used in the presentation of the crystal data. The molecular conformation and geometry were studied through MOGUL [31], a knowledge base that take a molecule submitted either manually or by another computer program via an instruction-file interface and perform substructure searches of the Cambridge Structural Database (CSD) [32] for, typically, all its bonds, angles, and torsional angles.

In spite of compound (I) crystallizing in a non-centrosymmetric space group, the Flack parameter was not refined during X-ray crystallographic analysis. Since the most electron-rich atom is oxygen, which does not have an anomalous scattering large enough (using MoK_{α} radiation) to permit determination of the absolute structure using X-ray diffraction, Friedel pairs were averaged before refinement.

Compound (II) was identified with basis on their chromatographic and spectral data which were identical to those of epiclusianone standard previously featured by our research group through X-ray diffraction analysis and spectroscopic measurements (UV, IR, MS, NMR) [8,33].

2.4. Molecular calculations starting on XRD structures of compound (I) and clusianone

The calculations were performed on a two dual core 2-GHz Opteron processor PC computer running Fedora 7 Linux. The quantum calculations were carried out in the gas phase using a full *ab initio* Hartree-Fock methodology with the 6-31G** basis implemented in the GAMESS-US code [34,35]. As input, the geometries determined by the X-ray diffraction analysis were used without further optimization. The HOMO and LUMO orbitals, and the dipole moments for each structure were calculated as implemented in the GAMESS-US program. The graphical representations of the computed orbitals were generated using the program Jmol [36].

3. Results and discussion

In the HPLC analysis benzophenones (I) and (II) have shown, respectively, retention times of 16.08±0.13 and 17.94±0.06 min. The peaks of compounds (I) and (II) have a subtle shoulder on the tail, presenting an asymmetric shape, which can be probably caused by occurrence of two keto-enol tautomers from each compound [6]. In the chromatographic analysis carried out with **GBFHE** samples, a few peaks could be observed and the chromatogram interpretation was facilitated. At the retention times of compounds (I) and (II), no signal other than chemical background was observed. A linear relationship between the peak area ratios and dilution concentrations ranging from 0.5 to 40 mg L^{-1} is confirmed by the mean correlation coefficients of 0.999±0.001 for compound (I) and 0.998±0.008 for benzophenone (II). The linear equations of compounds (I) and (II)

were respectively $y = (0.015\pm0.002)x - 0.015\pm0.008$ and $y = (0.012\pm0.002)x + 0.016\pm0.011$. Using these equations and the peak area ratios obtained in **GBFHE** samples analyses, we have found the amounts of 25±2 mg of compound (I) and 263±40 mg of substance (II) *per* g of **GBFHE**, stating that the tetraprenylated benzophenone (II) is a major compound from the *G. brasiliensis* fruits.

With regard to XRD analysis, as can be seen in Fig. 1, an ORTEP-3 [29] representation, the title compound does not contain a prenyl group attached at C5. It is very important to emphasise that garciniaphenone (I) is the first one in the respective class of related polyprenylated benzophenones without a C5 prenyl substituent. This feature is the unique difference between compounds (I) and (II). The stereochemistry around C7 atom is also the same in benzophenones (I) and (II), and the prenyl group atoms (C24 to C28) are above the plane passing through atoms C1, C5 and C7, in an axial orientation. This configurational feature causes other similarities between these two structures: The occurrence of the C10=O2/C4-O1-H1 tautomer in the solid state and the spatial orientation of the benzoyl group on the C3-C10 bond axis. The axial position of prenyl group connects the C25=C26 and C2=O3 groups, facilitating an intramolecular dipolar interaction between such ones [11]. The intramolecular distances from the centroid calculated between C25 and C26 atoms to the O3 atom are 3.455(3) Å in compound (I) and 3.734(4) Å in benzophenone (II) (Santos et al., 1998). In both the before mentioned cases such distances are concordant with the expected ones for the formation of an intramolecular contact mentioned. In view of the dipolar contact, the C2=O3 carbonyl group acting as electronic donor to C25=C26 group remains with electronic default, which deviates the covalent hydrogen bond to O1 atom. Therefore, the molecular stabilization occurs by O1-H1…O2 H-bond that forces the rotation on C3-C10 axis. This influence of C7 stereochemistry is proved viewing the clusianone [22], the epimer of compound (II) (Scheme 2), for which

the benzoyl group is rotated about 180° around C3-C10 axis in comparison with structures (I) and (II). In this case, the equatorial orientation of C24-C28 prenyl group (below C1-C5-C7 plane) keeps the double bond at C25 carbon far away from the C2 carbonyl group (distance between C25-C26 centroid and O3 is 5.321 Å). Contrasting to structures (I) and (II), the intramolecular interaction is hindered and as a result the default in the electronic density is not achieved in O3 atom, allowing the OH covalent bond to occur at O3 atom and subsequent benzoyl group rotation in order to stabilize the structure via O3-H1…O2 H-bond.

Scheme 2
Figure 1

We have performed *ab initio* calculations in search of theoretical approaches that could explain some of the structural features pointed out by XRD analysis. In Table 2, overall energy content, the HOMO, LUMO and HOMO-LUMO gap energies, and the dipole moment (μ) are displayed for compound (I) and clusianone. Analyzing these quantum-chemical values, it can be noted that all physical descriptors, except the dipole moment (μ), are similar for the two benzophenones. The difference between the μ values of compounds (I) and clusianone is expected, taking in account that the compound (I) does not show a prenyl group bonded to C5 atom. However, a very interesting data are illustratively shown in Fig. 2, a representation of LUMO frontier molecular orbital surfaces for natural product (I) and clusianone. In this depiction, it can be observed that on the C25 and C26 atoms of compound (I), which are doubly bonded and compose the prenyl group involved in the configuration of C7, the partial contribution in the LUMO orbital is higher than the respective one calculated for clusianone, although the highest coefficients of this

frontier molecular orbital for both compounds are on the carbon atoms of the unsaturation found in the prenyl moiety including from C19 to C23 atoms. This bulkier participation of C25=C26 in the overall LUMO orbital of compound (I) in comparison to clusianone reveals an enhanced electronic affinity [37] in these two carbon atoms where the prenyl group is axially oriented on C7, as it is reported for compound (I) in this paper. On the other hand, in the case of clusianone, the lowered coefficient on such double bond for LUMO content and consequently a minor electrophilic character of these related atoms are associated with the opposed stereochemistry of C24-C28 prenyl substituent on the chiral C7 atom. These theoretical findings are fitted to the before mentioned XRD evidences stating an intramolecular interaction between C25=C26 and C2=O3 groups of (I), which decreases the nucleophilic potential of the query oxygen atom to bond hydrogens, due to electronic donation from the O3 to the two sp^2-hybridized carbons. The electronic acceptance of C25=C26 is verified by the high electrophilicity in these atoms, which was computationally highlighted using LUMO calculations.

Table 2

Figure 2

The phenyl ring has presented bond angles and distances in agreement with the expected ones (C-C distances mean 1.37(3) Å and C-C-C angles mean 120.0(16)°), with individual values for angles and distances highly similar. This ring, as expected, is planar and the largest deviation from the least-squares plane through the six ring C atoms is 0.031(7) Å for C14 atom (Rms deviation of fitted atoms = 0.0185 Å). The carbonyl C10=O2 group is non-conjugated with the phenyl ring due to the reduced planarity between query groups. This fact can be noted by the highlighted deviation from the phenyl

ring least-squares plane for O2 atom, -0.830(7) Å, and by the torsional angle between C10=O2 group and the aromatic plane, 43.7(3)°. On the other hand, the C10=O2 group participates of a chelating six-membered cyclic system electronically delocalized, formed by O2-C10-C3-C4-O1-H1 atoms, which is almost entirely planar in view of the highest deviation from the least-squares plane passing through aforementioned six cyclic atoms to be -0.043(3) Å for C10 (Rms deviation of fitted atoms = 0.0466 Å). Furthermore, the intramolecular geometry in the chelating group, as well as the geometry from whole molecule, was analyzed using MOGUL [31], and this assessment have confirmed the delocalized resonant character in this system by the variations in the valence angles and bond distances (Tables 3 and 4). The single bonds C3-C10 (1.425(4) Å) and O1-C4 (1.285(3) Å) are markedly shorter than the average query values, respectively equal to 1.48(3) and 1.32(3) Å, whereas the double bond O2=C10 (1.270(4) Å) is longer than the value 1.22(2) Å averaged on 2995 hits containing structures similar to compound (I), and that were searched by MOGUL in the Cambridge Structural Database (CSD) [32]. These deviations from the most common bond distance values have been seen as result of entire electronic delocalization through the atoms O2-C10-C3-C4-O1-H1 that in solution leads to two tautomers depicted in Scheme 1. The previous observation allows us to state that C3-C10 and O1-C4 single bonds possess a character of double one and that O2=C10 double one presents single bond feature. Furthermore, the hydroxylic type of carbonyl C10=O2 group in the hybrid resonance structure can be also noted by the enlargement on the C3-C10-C11 valence angle, which supports the C10=O2 group. The former (124.3(3)°) is raised when compared to the average angles whose the corner C atom is carbonylic (120(2)°). In turn, the angle adjoining to C3-C10-C11, O2-C10-C11, is contracted. This angle value is 116.6(3)°, whereas the mean value for similar entries in CSD is 120(2)°. The intramolecular hydrogen bond O1-H1...O2 also disturbs the valence angles of the hybrid

keto-enol cyclic system, acting in a manner similar to C3-C10-C11 enhancement. The closeness between the C10=O2 and C4-O1 groups due to intramolecular hydrogen bond, which is viewed in Table 5 by the relatively short intramolecular O1…O2 distance (2.409 (4) Å), have centripetally positioned the C3-C10 bond in the direction of the de H-bonded cycle. As expected for this independent displacement, there is no change in the O2-C10-C3 angle (query value of 119.0 (3)° in compound (I) and average one of 119 (2)° for 161 (I)-like entries in CSD), whereas the angles C2-C3-C10 (123.0 (2)°) and C4-C3-C10 (117.9 (2)°) have been consequently relaxed and constrained, respectively, in comparison with the mean values (119 (3)° for C2-C3-C10 and 121 (2)° for C4-C3-C10).

Tables 3 and 4

In guttiferone A, a benzophenone structurally related to compound (I) that is present in the *G. brasiliensis* seeds, the hydroxyl group in *para*-position from aromatic ring origins a further delocalized resonance path along the atoms OH_p-Ph-C11-C10-O2 that enhances the electronic density around O2 atom [11]. In view of that, the O2 atom become covalently bonded to H1 and the keto-enol C10-O2-H1/C4=O1 tautomer was found to have the highest relative contribution in solid state of guttiferone A, differently from C10=O2/C4-O1-H1 one determined here in (I) crystal structure.

In the bicyclic system, the six-membered rings C5–C6-C7-C8-C1-C9 and C1–C2-C3-C4-C5-C9 take on chair and distorted half-chair conformations, respectively. The (I) bond length C5-C6 is 1.545(4) Å. This value is shorter than the equivalent C5-C6 distances from clusianone (1.603 Å) [22] and compound (II) [8]. The C5-C6 separation shortening has been caused by the decrease in the tension about the C-C bonds involving the C5 atom from compound (I), which follows the substitution degree reduction in this atom from (I)

in comparison to clusianone and compound (II). Additionally, the absence of a prenyl group on C5 atom is also responsible by the opening of O4-C9-C1 angle (124.9(3)°), which was greater than the query mean value (121(1)°). When present on C5 atom, the bulky prenyl group repulses sterically the carbonyl O4=C9 one and the last bond is strained in the direction of the C1-C9 bond spatial domain. Thereby, O4-C9-C1 angle is contracted and O4-C9-C5 one is expanded as consequence. As in compound (I) there is no a fourth substituent attached on C5 atom, as for instance a prenyl group typical of alike natural benzophenones, the steric hindrance not occurs and the O4-C9-C1 angle is released as described here. A slight closing in the O4-C9-C5 angle (121.6(3)°) was also verified with the searches carried out by MOGUL [31], whose average angle in query was 123(1)°, in agreement with the predicted angular deformations abovementioned.

The chelating system is stabilized through the intramolecular hydrogen bond O1-H1…O2 responsible by the benzoyl group rotation (Fig. 1, Table 5). Looking the intermolecular geometry, it is verified that compound (I) exhibits three non-classical intermolecular hydrogen bonds. Two of them, C14-H14…03 hydrogen bond, between the phenyl ring and the adjacent C2=O3 carbonyl group, and C8-H8b…O2 one, between the C8 atom from bicyclic ring and the C10=O2 carbonyl group belonging to benzoyl moiety, stabilize the molecules along the [100] direction, in a stacking form, forming an infinite ribbon in this direction (Fig. 3). Already the intermolecular C25-H25…O4 hydrogen bond, between the sp^2-hybridized C25 atom from the prenyl group including C24-C28 atoms and the carbonyl O4 atom, gives rise to a chain, in a zigzag molecular manner, parallel to the [010] direction (Fig. 4). Details of all intermolecular hydrogen bonds interactions involved in these networks are given in Table 5.

Figures 3 and 4

Table 5

4. Conclusions

The crystal structure of (I), the first compound in the respective class of analogous polyprenylated benzophenones without a C5 prenyl substituent, was determined for the fist time in this work, resulting in a correct characterization of the intra and inter-molecular geometries. In the solid state of benzophenone (I), C10=O2/C4-O1-H1 tautomer was found, in the same chemical form of related natural benzophenone (II) and differently from guttiferone A, a C10-O2-H1/C4=O1 tautomer as crystallographic independent molecule. Some changes in bond angles and lengths and torsional deviations were reported as consequence of a chelating delocalized six-membered system throughout O2-C10-C3-C4-O1-H1, likewise the substitution pattern on C5 atom has influenced the structural geometry in comparison with benzophenones that are more substituted at this atom. In addition, the reason for differential keto-enol tautomeric forms between compound (I) and clusianone can probably be in the stereochemistry of C7 atom, which was further strengthened by LUMO calculations performed comparatively with query compounds.

5. Supplementary material

Supplementary crystallographic data sets for (I) is available through the Cambridge Structural Data Base, deposition number CCDC 667556. Copies of this information may be obtained free of charge from The Director, CCDC, 12 Union Road, Cambridge, CB2

1EZ, UK (Fax: +44 123 336 033; e-mail: deposit@ ccdc.cam.ac.uk or http:www.ccdc.ac.uk).

Acknowledgements

We thank the Brazilian Research Council CNPq (Conselho Nacional de Desenvolvimento Científico e Tecnológico) and CAPES (Coordenação de Aperfeiçoamento de Pessoal de Nível Superior) for research fellowships (LCAB, ACD, JE, and FTM), FAPEMIG (Fundação de Amparo à Pesquisa do Estado de Minas Gerais Proc.: EDT-3310/06) and FINEP (Financiadora de Estudos e Projetos – Proc.: 1110/06) for financial support, and Instituto Rocasolano-CSIC, Spain, for the CSD licence.

References

[1] M. P. Corrêa, Dicionário das plantas úteis do Brasil e das plantas exóticas cultivadas, Imprensa Nacional, Rio de Janeiro, 1978.

[2] G.D. Monache, B. Botta, J.F. Mello, J.S.B. Coelho and F. Menichini, J. Nat. Prod., 47 (1984) 620.

[3] G.J. Bennett and H.H. Lee, Phytochemistry, 28 (1989) 967.

[4] E.G. Crichton and P.G. Waterman, Phytochemistry, 18 (1979) 1553.

[5] A.A.L. Gunatilaka, S. Sotheeswaran, H.T.B. Sriyan and E.S. Waight, Tetrahedron Lett., 23 (1982) 2987.

[6] O.C. Rubio, A. Padron, H.V. Castro, C. Pizza and L. Rastrelli, J. Nat. Prod., 64 (2001) 973.

[7] B. Botta, M.M. McQuhae, G.D. Monache, F.D. Monache and J.F. Mello, J. Nat. Prod., 47 (1984) 1053.

[8] M.H. Santos, N.L. Speziali, T.J. Nagem and T.T. Oliveira, Acta Crystallogr., C54 (1998) 1990.

[9] K.R. Gustafson, J.W. Blunt, H.G.M. Munro, R.W. Fuller, C.T. McKee, J.H. Cardellina, J.B. McMahon, G.M. Cragg and M.R. Boyd, Tetrahedron, 48 (1992) 10093.

[10] B.N. Lenta, D.T. Noungoue, K.P. Devkota, P.A. Fokou, S. Ngouela, E. Tsamo and N. Sewalda, Acta Crystallogr., E63 (2007) 1282.

[11] F.T. Martins, J.W. Cruz JR., P.B.M.C. Derogis, M.H. Santos, M P. Veloso, J.A. Ellena and A.C. Doriguetto, J. Braz. Chem. Soc., in press (2007).

[12] F. Abe, S. Nagafuji, H. Okabe, H. Akahane, E.E. Muñiz, M.H. Reyes and R.R. Chilpa, Biol. Pharm. Bull., 27 (2004) 141.

[13] M.H. Pan, W.L. Chang, S.Y. Lin-Shiau, C.T. Ho and J.K. Lin, J. Agric. Food Chem., 49 (2001) 1464.

[14] T. Tanaka, H. Kohno, R. Shimada, S. Kagami, F. Yamaguchi, S. Kataoka, T. Ariga, A. Murakami, K. Koshimizu and H. Ohigashi, Carcinogenesis, 21 (2000) 1183.

[15] F. Yamaguchi, T. Ariga, Y. Yoshimura and H. Nakazawa, J. Agric. Food Chem., 48 (2000) 180.

[16] F. Yamaguchi, M. Saito, T. Ariga, Y. Yoshimura and H. Nakazawa, J. Agric. Food Chem., 48 (2000) 2320.

[17] C. Gopalakrishnan, D. Shankaranarayan, S.K. Nazimudeen and L. Kameswaran, Ind. J. Med. Res., 71 (1980) 940.

[18] D.D. Carballo, S. Seeber, D. Strumberg and R.A. Hilger, Int. J. Clin. Pharm. Th., 41 (2003) 622.

[19] A.J. Cruz, V.S. Lemos, M.H. Santos, T.J. Nagem and S.F. Cortes, Phytomedicine, 13 (2006) 442.

[20] A.L. Piccinelli, O.C. Rubio, M.B. Chica, N. Mahmood, B. Pagano, M. Pavone, V. Barone and L. Rastrelli, Tetrahedron, 61 (2005) 8206.

[21] P.B.M.C. Derogis, F.T. Martins, T.C. Souza, M.E.C. Moreira, J.D. Souza Filho, A.C. Doriguetto, K.R. Souza, M.P. Veloso and M.H. Santos, Magn. Reson. Chem., in press (2007).

[22] L.E. McCandlish, J.C. Hanson and G.H. Stout, Acta Crystallogr., B32 (1976) 1793.

[23] A.C. Doriguetto, F.T. Martins, J.A. Ellena, R. Salloum, M.H. Santos, M.E.C. Moreira, J.M. Schneedorf and T. J. Nagem, Chem. Biodiversity, 4 (2007) 488.

[24] Enraf-Nonius *COLLECT*. Nonius BV, Delft, The Netherlands, 1997–2000.

[25] Z. Otwinowski, W. Minor, in: C.W. CarterJr., R.M. Sweet (Eds.), Methods in Enzymology, vol. 276, Academic Press, New York, 1997, p. 307.

[26] G.M. Sheldrick, *SHELXS-97*. Program for Crystal Structure Resolution, University of Göttingen, Göttingen, Germany, 1997.

[27] G.M. Sheldrick, *SHELXL-97*. Program for Crystal Structures Analysis, University of Göttingen, Göttingen, Germany, 1997.

[28] L.J. Farrugia, J. Appl. Cryst., 32 (1999) 837.

[29] L.J. Farrugia, J. Appl. Cryst., 30 (1997) 565.

[30] I.J. Bruno, J.C. Cole, P.R. Edgington, M.K. Kessler, C.F. Macrae, P. McCabe, J. Pearson and R. Taylor, Acta Crystallogr., B58 (2002) 389.

[31] I.J. Bruno, J.C. Cole, M. Kessler, J. Luo, W.D.S. Motherwell, L.H. Purkis, B.R. Smith, R. Taylor, R.I. Cooper, S.E. Harris and A.G. Orpen, J. Chem. Inf. Comput. Sci., 44 (2004) 2133.

[32] F.H. Allen, Acta Crystallogr., B58 (2002) 380.

[33] M.H. Santos, T.J. Nagem, R. Braz-Filho, I.S. Lula and N.L. Speziali, Magn. Reson. Chem., 39 (2001) 155.

[34] M.W. Schmidt, K.K. Baldridge, J.A. Boatz, S.T. Elbert, M.S. Gordon, J.H. Jensen, S. Koseki, N. Matsunaga, K.A. Nguyen, S.J. Su, T.L. Windus, M. Dupuis and J.A. Montgomery, J. Comput. Chem., 14 (1993) 1347.

[35] M.S. Gordon and M.W. Schmidt, in C.E. Dykstra, G. Frenking, K.S. Kim and G.E. Scuseria (Eds.), Advances in electronic structure theory: GAMESS a decade later, Theory

and Applications of Computational Chemistry: The first forty years, Elsevier, Amsterdam, 2005.

[36] Jmol: an open-source Java viewer for chemical structures in 3D. http://www.jmol.org/.

[37] A. Modelli and L. Mussoni, Chem. Phys., 332 (2007) 367.

Table 1. Crystal data and structure refinement for compound (I).

Empirical formula	$C_{28}H_{34}O_4$
Formula weight	434.55
Temperature [K]	293(2)
Wavelength [Å]	0.71073
Crystal system	Orthorhombic
Space group	$P\,2_12_12_1$
Unit cell dimensions	a =8.9985(3) Å α=90.000(2)°
	b=14.4589(6) Å β=90.000(2)°
	c=18.4322(6) Å γ=90.000(3)°
Volume [Å^3]	2398.2(1)
Z	4
Density (calculated) [Mg/m^3]	1.204
Absorption coefficient [mm^{-1}]	0.079
F(000)	936
Crystal size [mm]	0.1 x 0.2 x 0.4
θ-Range for data collection [°]	3.03-28.12
Index ranges	$-11 \le h \le 11$; $-18 \le k \le 18$; $-22 \le l \le 23$
Reflections collected	20638
Independent reflections	3110 [R(int) = 0.0407]
Completeness to θ=28.12°	94.2 %
Refinement method	Full-matrix least-squares on F^2
Data/restraints/parameters	3110 / 0 / 294
Goodness-of-fit on F^2	1.045
Final R for $I>2\sigma(I)$	$R1$=0.0556
R indices (all data)	$wR2$=0.1803
Largest diff. peak and hole [e.Å^{-3}]	0. 246, -0.187

Table 2. Values of some quantum-chemical properties calculated for compound (I) and clusianone.

	(I)	*clusianone*
E (Hartree)	-1379.06	-1573.17
E_{HOMO} (eV)	-8,74	-8,81
E_{LUMO} (eV)	1,95	1,93
$E_{HOMO\text{-}LUMO\ gap}$ (eV)	10,69	10,78
μ (Debye)	2.81	1.54

Table 3. Bond lengths in Å of compound (I) determined by XRD (query value) and MOGUL intramolecular analysis

Fragment	Number	Mean	Query value
C(1)-C(2)	7	1.51(1)	1.527(4)
C(2)-C(3)	103	1.44(2)	1.472(4)
C(3)-C(4)	18	1.39(2)	1.405(4)
C(4)-C(5)	2	1.52(1)	1.497(4)
C(5)-C(6)	7	1.55(1)	1.545(4)
C(6)-C(7)	22	1.54(1)	1.545(4)
C(7)-C(8)	271	1.53(1)	1.530(4)
C(1)-C(8)	59	1.53(1)	1.516(4)
C(1)-C(9)	15	1.53(1)	1.492(4)
C(1)-C(19)	76	1.55(4)	1.525(4)
C(3)-C(10)	**161**	**1.48(3)**	**1.425(4)**
C(5)-C(9)	9	1.51(1)	1.495(4)
C(6)-C(17)	3573	1.52(3)	1.516(4)
C(6)-C(18)	3573	1.52(3)	1.537(4)
C(7)-C(24)	24	1.54(1)	1.503(4)
C(10)-C(11)	915	1.48(3)	1.471(5)
C(11)-C(12)	10000	1.38(1)	1.358(7)
C(12)-C(13)	10000	1.38(2)	1.395(10)
C(13)-C(14)	10000	1.37(3)	1.29(2)
C(14)-C(15)	10000	1.37(2)	1.426(16)
C(15)-C(16)	10000	1.38(2)	1.374(6)
C(11)-C(16)	10000	1.38(1)	1.362(8)
C(24)-C(25)	171	1.49(2)	1.497(4)
C(25)-C(26)	361	1.31(3)	1.319(5)
C(26)-C(27)	1140	1.49(3)	1.500(5)
C(26)-C(28)	1140	1.49(3)	1.480(6)
C(19)-C(20)	152	1.49(3)	1.485(5)
C(20)-C(21)	361	1.31(3)	1.309(5)
C(21)-C(22)	1140	1.49(3)	1.458(6)
C(21)-C(23)	1140	1.49(3)	1.494(6)
O(1)-C(4)	**105**	**1.32(3)**	**1.285(3)**
O(2)-C(10)	**2995**	**1.22(2)**	**1.270(4)**
O(3)-C(2)	1225	1.21(2)	1.203(3)
O(4)-C(9)	1247	1.20(2)	1.203(4)

Table 4. Bond Angle [°] of compound (I) determined by XRD (query value) and MOGUL intramolecular analysis.

Fragment	Number	Mean	Query value
C(1)-C(2)-C(3)	19	119(2)	118.0(2)
C(1)-C(8)-C(7)	7	114(1)	117.5(2)
C(1)-C(9)-C(5)	16	116(2)	113.5(3)
C(1)-C(19)-C(20)	27	113(2)	112.3(3)
C(2)-C(1)-C(8)	15	108(1)	108.4(2)
C(2)-C(1)-C(9)	23	111(3)	110.3(2)
C(2)-C(1)-C(19)	9	109(2)	109.4(2)
C(2)-C(3)-C(4)	15	120(1)	118.4(2)
C(2)-C(3)-C(10)	**15**	**119(3)**	**123.0(2)**
C(3)-C(4)-C(5)	15	119(4)	122.3(2)
C(3)-C(10)-C(11)	**147**	**120(2)**	**124.3(3)**
C(4)-C(3)-C(10)	**15**	**121(2)**	**117.9(2)**
C(4)-C(5)-C(6)	2	113.7(2)	116.7(3)
C(4)-C(5)-C(9)	68	107(3)	107.2(2)
C(5)-C(6)-C(7)	24	107(2)	110.9(2)
C(5)-C(6)-C(17)	14	109(2)	109.3(2)
C(5)-C(6)-C(18)	14	109(2)	107.3(3)
C(6)-C(5)-C(9)	149	110(2)	108.2(2)
C(6)-C(7)-C(8)	4	110(1)	112.0(2)
C(6)-C(7)-C(24)	6	115(1)	113.7(2)
C(7)-C(6)-C(17)	44	109(2)	114.0(3)
C(7)-C(6)-C(18)	44	109(2)	108.1(3)
C(7)-C(24)-C(25)	18	114(3)	113.1(3)
C(8)-C(1)-C(9)	33	107(2)	105.7(2)
C(8)-C(1)-C(19)	7	111(1)	109.0(2)
C(8)-C(7)-C(24)	7	109(1)	114.3(2)
C(9)-C(1)-C(19)	27	108(2)	113.9(3)
C(10)-C(11)-C(12)	1762	120(2)	119.4(5)
C(10)-C(11)-C(16)	1762	120(2)	120.6(4)
C(11)-C(12)-C(13)	10000	120(1)	117.7(8)
C(11)-C(16)-C(15)	10000	120(1)	122.4(7)
C(12)-C(11)-C(16)	10000	118(1)	119.8(5)
C(12)-C(13)-C(14)	10000	120(1)	123.3(11)
C(13)-C(14)-C(15)	10000	120(2)	120.1(7)
C(14)-C(15)-C(16)	10000	120(1)	116.3(9)
C(17)-C(6)-C(18)	510	107(1)	106.9(3)
C(24)-C(25)-C(26)	26	128(2)	126.9(3)
C(25)-C(26)-C(27)	722	122(3)	120.1(4)
C(25)-C(26)-C(28)	722	122(3)	124.8(4)
C(27)-C(26)-C(28)	570	114(2)	115.0(4)
C(19)-C(20)-C(21)	73	128(4)	127.3(4)
C(20)-C(21)-C(22)	722	122(3)	121.7(4)
C(20)-C(21)-C(23)	722	122(3)	122.7(4)
C(22)-C(21)-C(23)	570	114(2)	115.5(4)
O(1)-C(4)-C(3)	18	122(1)	122.0(3)
O(1)-C(4)-C(5)	18	113(3)	115.7(2)
O(2)-C(10)-C(3)	161	119(2)	119.0(3)
O(2)-C(10)-C(11)	**915**	**120(2)**	**116.6(3)**
O(3)-C(2)-C(1)	7	119(2)	119.0(2)
O(3)-C(2)-C(3)	103	123(2)	123.0(3)

O(4)-C(9)-C(1)	**15**	**121(1)**	**124.9(3)**
O(4)-C(9)-C(5)	9	123(1)	121.6(3)

Table 5. Hydrogen-bonding length (A°) and angles (°) of compound (I). *'D' and 'A' mean hydrogen donor and acceptor, respectively.*

D - H...A	D - H	H...A	D...A	D - H...A
O1 - H1...O2	1.06(5)	1.40(6)	2.409(4)	156(5)
C8 - H8B...O2[a]	0.97	2.60	3.515(4)	158
C14 - H14...O3[b]	0.93	2.53	3.414(8)	159
C25 - H25...O4[c]	0.93	2.74	3.632(5)	161
C28 - H28C...O3	0.96	2.57	3.351(5)	139

[a]: 1+x, y, z; [b]:-½+x, ½-y, -z; [c]: 2-x; -½+y; ½-z

Scheme 1. Keto-enol tautomers of compound (I) at $CDCl_3$ solution [21] showing the same C-atom labelling used for XRD structural representation.

Scheme 2. Compound (II) and its epimer, clusianone, as major tautomeric forms.

Figure 1. ORTEP view of compounds (I) and (II) [8] showing the arbitrary atom labelling. Ellipsoids represent 50% probability level. Double dotted lines represent either the intramolecular hydrogen bond or the dipolar interaction between the C25=C26 and C2=O3 groups. The C-H H-atoms were omitted for clarity.

Figure 2. Representation of the coefficients for overall LUMO orbital of compound (I) and clusianone.

Figure 3. Crystal packing view of compound (I) along the [100] direction. Double dotted lines represent hydrogen bonds. The H-atoms involved in the hydrogen bonds are shown as spheres of arbitrary radii. *Symmetry codes:* (*i*) x + ½; - y + ½; -z; (*ii*) x - ½; - y + ½; -z.

Figure 4. Crystal packing view of compound (I) along the [010] direction. Double dotted lines represent hydrogen bonds. The H-atoms involved in the hydrogen bonds are shown as spheres of arbitrary radii. *Symmetry codes:* (*i*) -x + 2; y + ½; -z + ½; (*ii*) -x + 2; y - ½; -z + ½.

Scheme 1

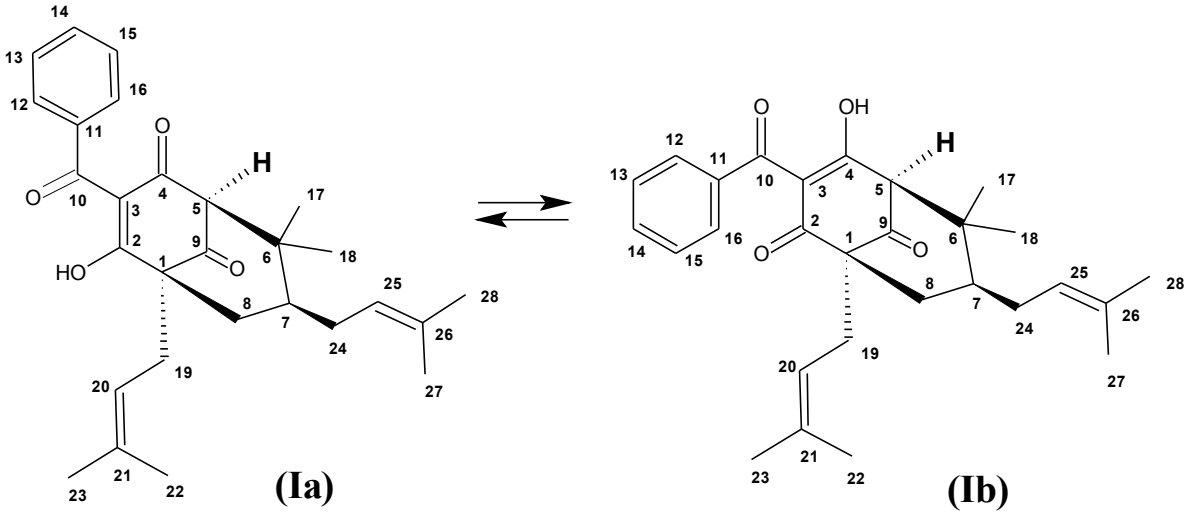

Scheme 2

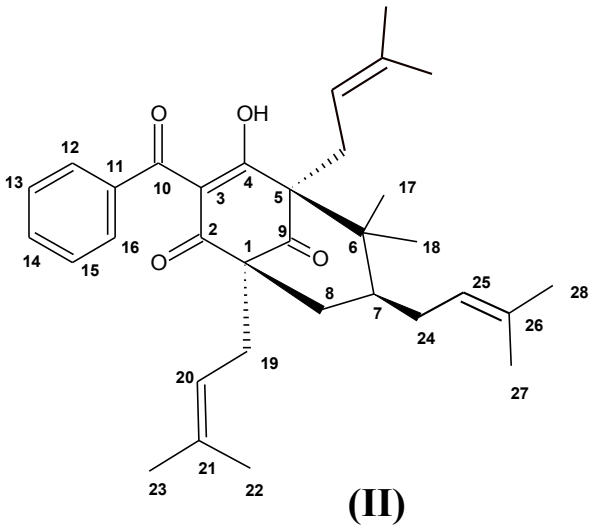

(II)

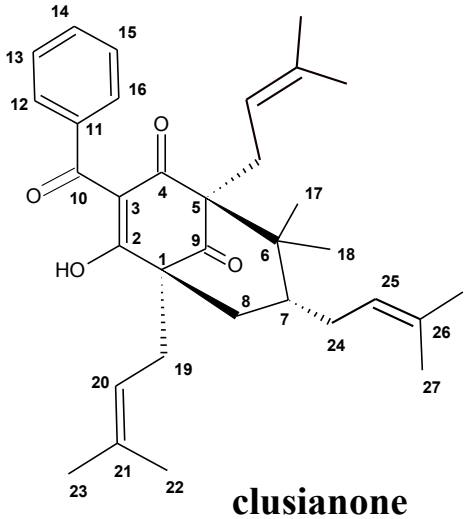

clusianone

Figure 1

(I)

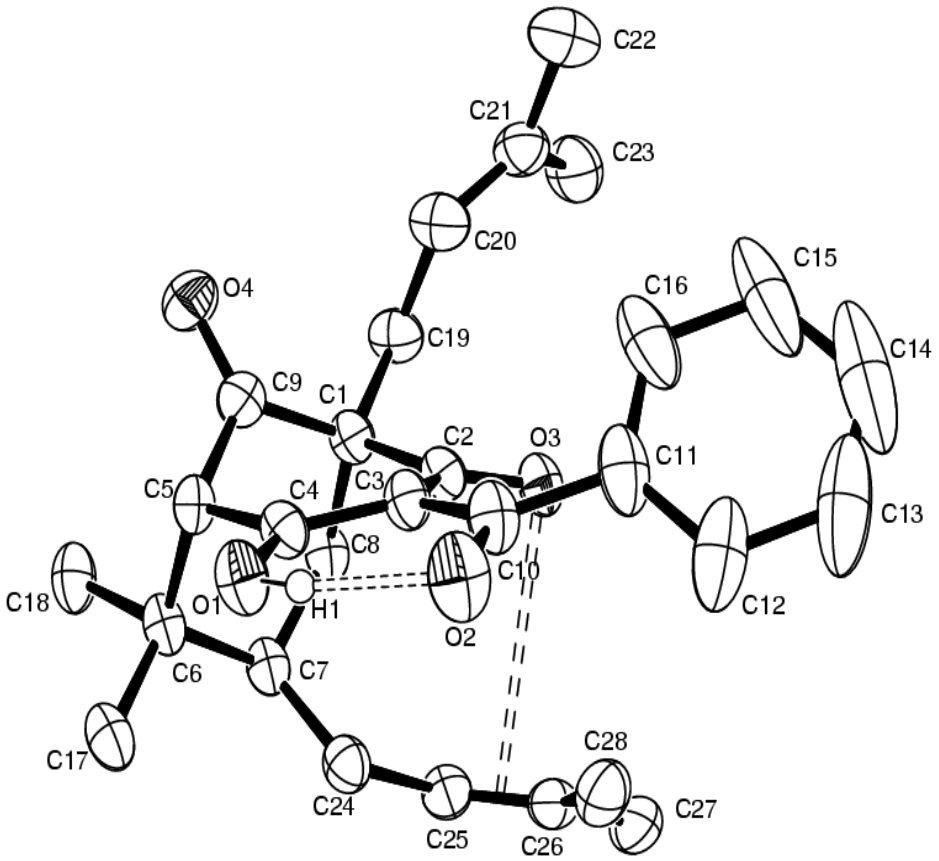
C22
C21
C23
C20
C15
C16
O4
C19
C14
C9
C1
C2
O3
C11
C5
C4
C3
C13
C8
C10
C18
O1
H1
O2
C12
C6
C7
C17
C28
C24
C27
C25
C26

(II)

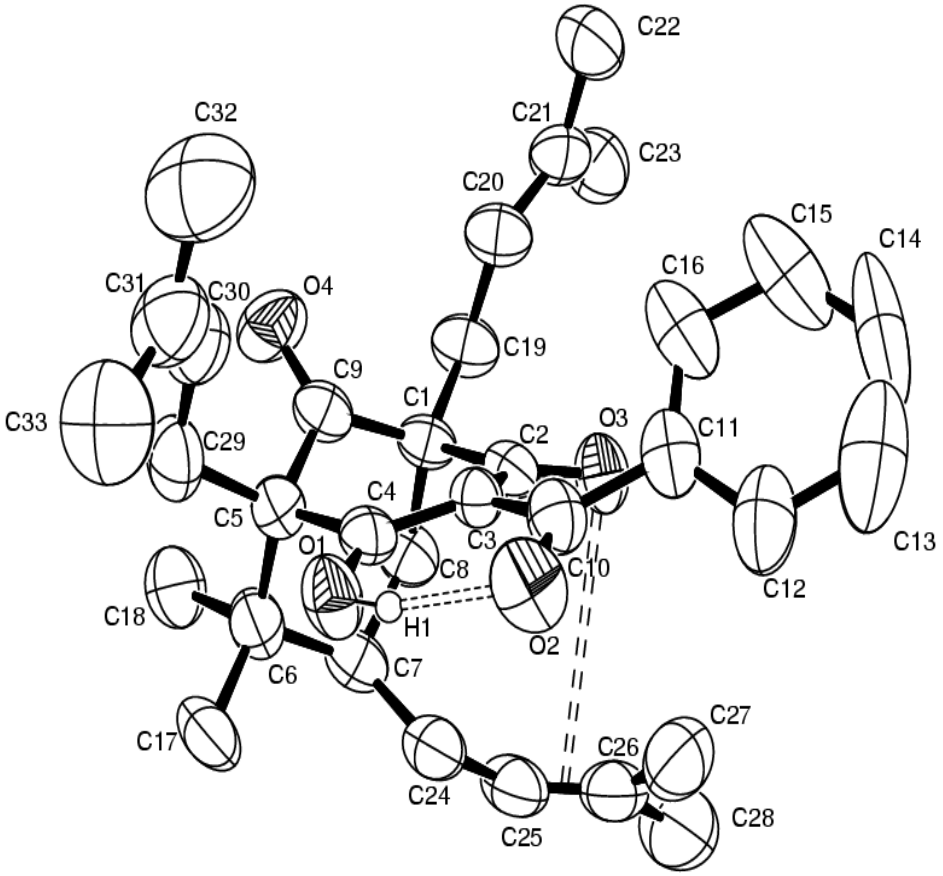
C22
C32
C21
C23
C20
C15
C14
C16
C31
C30
O4
C19
C9
C1
C33
C29
C2
O3
C11
C4
C5
C3
O1
C13
C8
C10
C12
C18
H1
O2
C6
C7
C27
C17
C26
C24
C28
C25

Figure 2

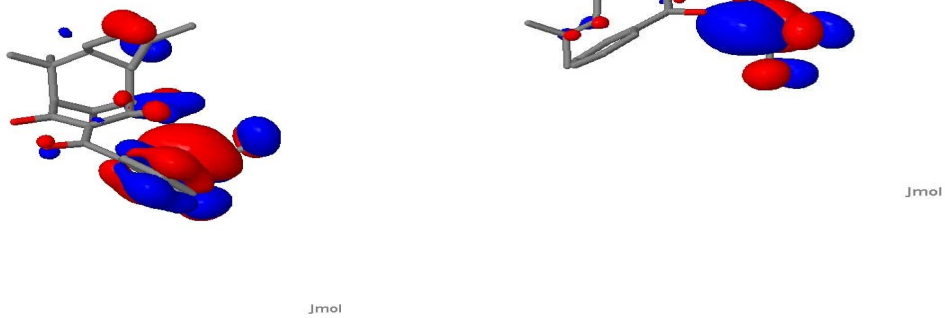

(I) **clusianone**

Figure 3

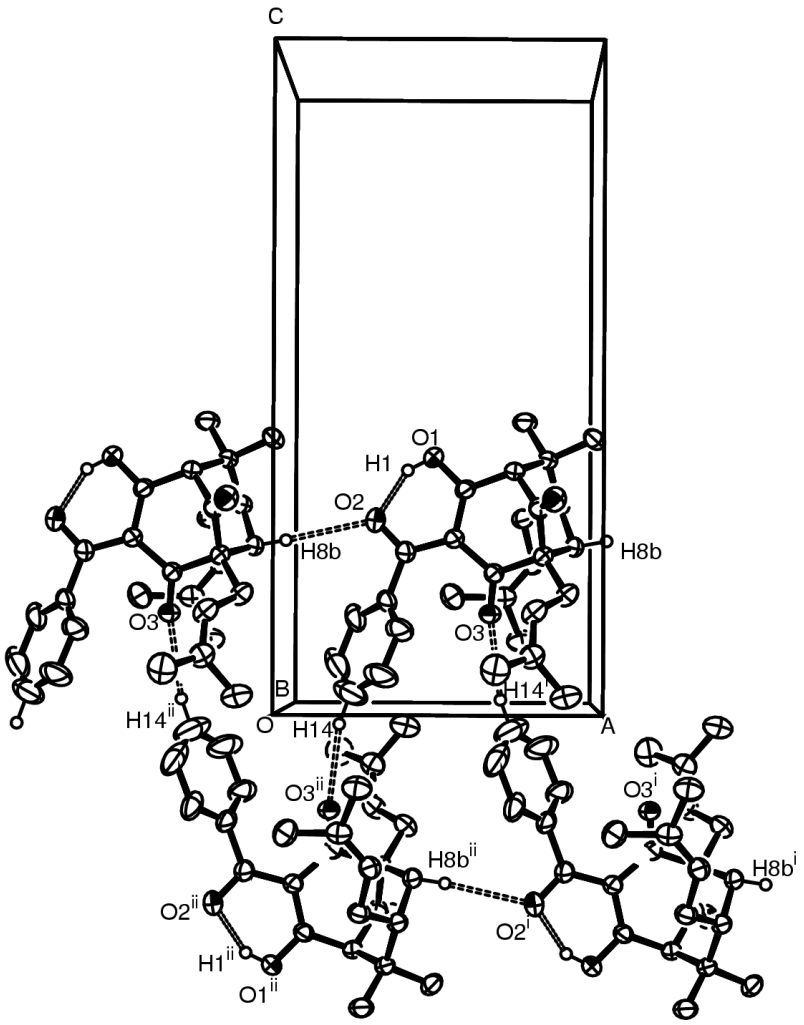
C
O1
H1
O2
H8b
H8b
O3
O3
B
H14^{i}
H14^{ii}
O
H14
A
O3^{ii}
O3^{i}
H8b^{ii}
H8b^{i}
O2^{ii}
O2^{i}
H1^{ii}
O1^{ii}

Figure 4

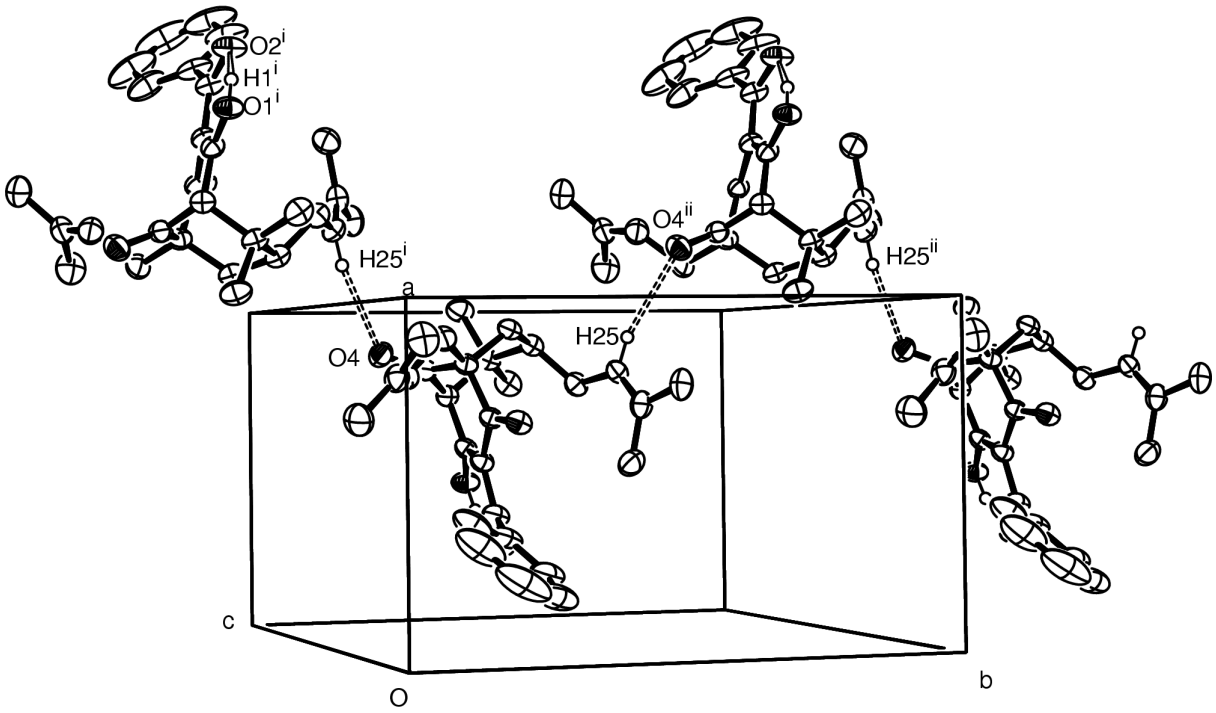

4 PARTE 2: ATIVIDADE ANTIPROTEOLÍTICA DE BENZOFENONAS NATURAIS E SINTÉTICAS

4.1 "NATURAL POLYPRENYLATED BENZOPHENONES INHIBITING CYSTEINE AND SERINE PROTEASES"

MARTINS, F. T., ASSIS, D. M., SANTOS, M. H., CAMPS, I., VELOSO, M. P., JULIANO, M. A., ALVES, L. C., DORIGUETTO, A. C. Natural polyprenylated benzophenones inhibiting cysteine and serine proteases. **European Journal of Medicinal Chemistry**. *submitted*, 2007.

Natural polyprenylated benzophenones inhibiting cysteine and serine proteases

Felipe T. Martins*[,a], Diego M. Assis[a], Marcelo H. dos Santos[a], I. Camps[a], Márcia P. Veloso[a], Maria A. Juliano[b], Lira C. Alves[a], Antônio C. Doriguetto[a]

[a] *Department of Exact Science, Federal University of Alfenas, Rua Gabriel Monteiro da Silva 714, Alfenas - MG, 37130-000, Brazil*

[b] *Department of Biophysics, Federal University of São Paulo, Rua Três de Maio 100, São Paulo - SP, 04044-020, CP 369, Brazil*

∗ Corresponding to: Felipe T. Martins, Department of Exact Science, Federal University of Alfenas, Rua Gabriel Monteiro da Silva 714, Alfenas - MG, 37130-000, Brazil. E-mail: felipetmartins@yahoo.com.br; phone: +55-35-32991261; fax: +55-35-32991262.

Abbreviations: CC, column chromatography; TLC, thin layer chromatography; MAP, mitogen-activated protein; XRD, X-ray diffraction; HPLC, High Performance Liquid Chromatography; Z-FR-AMC, carbobenzyloxy-Phe-Arg-(7-amino-4-methylcoumarin); EDTA, ethylenediaminetetraacetic acid; DMSO, dimethyl sulfoxide; DTT, dithiothreitol; LP, leupeptin; E-64, 1-[[(L-*trans*-epoxysuccinyl)-L-leucyl]amino]-4-guanidinobutane; SBTI, soybean trypsin inhibitor; Abz-, *ortho*-aminobenzoic acid; -EDDnp, N-(ethylenediamine)-2,4-dinitrophenyl amide; IC_{50}, inhibitor concentration to decrease 50% enzymatic activity; VDW, van der Waals.

Abstract

We have investigated the in vitro inhibition of papain, trypsin, and cathepsins B and G by five benzophenone-type compounds, three natural ones isolated from *Garcinia brasiliensis* and two synthetic derivatives. The activities of pentaprenylated dihydroxy-substituted benzophenone guttiferone A (**1**) on all assayed enzymes were approximately 2-69 folds higher than that manifested by non-hydroxylated tetraprenylated and triprenylated compounds epiclusianone (**2**) and garciniaphenone (**3**), respectively, which are the other natural benzophenones that also inhibited significantly the four enzymes. Differently, the synthetic derivatives 2,2',4-trihydroxybenzophenone (**4**) and diphenylmethanone (**5**) have inhibited weakly the studied proteases. Furthermore, the compound **1** has bonded preferentially to cathepsin G, once its IC_{50} value (2.7±0.1 μM) on such peptidase is quite similar to that of the classical inhibitor of serine proteases, chymostatin (2.1±0.1μM). Interesting structure-activity relationships (SARs) were confirmed by flexible docking simulations, likewise the potential usefulness of natural compound **1** as antitumoral drug is strengthened by our results concerning the antiproteolytic activity.

Keywords: benzophenones; proteases; guttiferone A; Cathepsin G; SAR; flexible docking.

1. Introduction

Proteases or peptidases are enzymes that catalyze reactions on peptide chains. These enzymes can be further joined according to the reactant groups that are present in the catalytic site, as the serine (EC 3.4.21), cysteine (EC 3.4.22), aspartic (EC 3.4.23) and metalo proteases (EC 3.4.24). Papain (EC 3.4.22.2), a plant cysteine protease isolated from *Carica papaya* latex, is a 23 kDa single polypeptide chain containing 212 amino acid residues and three disulfide bonds (Cys22-Cys63, Cys56-Cys95, and Cys153-Cys200). This protease cleaves preferentially peptides chains on either Arg and Lys residues or hydrophobic Phe ones. The recognition site that interacts with Phe residues is a hydrophobic pocket formed by the Trp69, Tyr67, Phe207, Pro68, Ala160, Val133 and Val157 moiety [1]. The cathepsins, a group of lysosomal enzymes, are proteases presenting several members. Two of them, cathepsin B (CatB, EC 3.4.22.1) and cathepsin G (CatG, EC 3.4.21.20) have been identified in human tissues, where they can be isolated. CatB, a 29 kDa glycoprotein, has a species-specific carbohydrate residue attached on either Asn110 or Asn113 ones [2]. This papain-like protease is barely detected in the extracellular matrix, at least in nonpathological tissues, due to its low stability in neutral-alkaline pH values [3,4]. It is interesting to note that the extracellular alkali-stable isoforms are more weighed than related lysosomal enzymes and they are mainly found in tumor tissues [1,3,5]. Concerning the neoplastic events, CatB is secreted out of the cells and it presents essentially an endopeptidase-functioned proteolytic activity crucial to tissue rupture around the tumor spreading area and metastasis [6,7]. Moreover, high expression, activity and secretion of CatB have been observed in several types of tumors, such as breast, gastric, lung and prostate ones [8]. The CatG is the major serine protease in the

azurophilic granules of polymorphonuclear leukocytes [9,10] and is involved in the degradation of foreign bodies and injured tissues enclosed by phagosomal vesicles during inflammatory responses [11]. In opposition to CatB, CatG is commonly released towards the extracellular matrix. Its proteolytic activity is finely controlled by serum proteinase inhibitors, which can fail quantitatively or qualitatively in down-regulation due to genetic or acquired deficiencies resulting in a disturbed digestion of extracellular proteins that could contribute to the development of connective tissue diseases, as emphysema, rheumatoid arthritis and perionditis [12]. In the way of the previous statement, the proteolyses of elastin, collagen type I and type II, cartilage proteoglycans, fibronectin, laminin and immunoglobulins G and M by CatG have been proved in vitro [12]. Furthermore, recent evidences have suggested that this lysosomal protease presents alternative physiologic roles, as for instance platelet activation [13], monocyte and neutrophil chemotaxis [14], natural killer cytotoxicity increasing [15], proteolytic processing of interleukin-8 [16], complement C3 [17] and factor V [18], as well as other pathological ones, such as dissemination of tumor aggregates from primary tumor sites after to be secreted out by infiltrated neutrophils [19].

Nevertheless, another important difference can be pointed out between CatG and CatB: the first one is chymotrypsin/trypsin-like protease, whereas the later is a papain-like enzyme. Trypsin (E.C. 3.4.21.4) has specificity for peptides containing Arg and Lys residues and its catalytic triad is composed by the amino acids serine, histidine and aspartate, in the same way that occurs in similar serine proteases [20].

Our research group has deal with synthetic and natural benzophenone derivatives regarding structural elucidation and screening for pharmacological properties on various biological systems. From the *G. brasiliensis* fruits and seeds, three benzophenones

possessing a polyprenylated bicycle[3.3.1]-nonane-2,4,9-trione core were isolated through repeated column chromatography (CC), repeated preparative thin layer chromatography (TLC) and recrystallizations in methanol solutions: guttiferone A (**1**), an anti-HIV compound that was initially isolated in 1992 [21]; epiclusianone (**2**), a vasoactive substance identified in 1998 [22] that also presents effects against HIV infection [23,24]; and garciniaphenone (**3**), a first example of natural benzophenone presenting just three prenyl moieties that has been discovered for the first time in this plant by us. A trihydroxylated benzophenone named systematically (2,4-dihydroxyphenyl)(2-hydroxyphenyl)methanone, or simply 2,2',4-trihydroxybenzophenone (**4**), was previously synthesized in our laboratories by aromatic electrophilic substitution [25]. All these benzophenone derivatives were spectroscopically featured and their structures have been accurately determined via single crystal X-ray diffraction crystallography [22,26,27], likewise the anti-inflammatory and antioxidant properties were recently described for such natural products [25]. Furthermore, the polyisoprenylated benzophenones derivative of the bicycle[3.3.1]-nonanetrione moiety are implicated in the inhibition of DNA topoisomerases and telomerase and also act as regulators within mitogen-activated protein (MAP) kinase signal transduction pathways, decreasing mitosis rate in cancerous and tumoral tissues, once MAP kinases are active enzymes during mitosis process [28]. Due to their merged effects on different pharmacological targets for antineoplastic therapy, the natural benzophenones in query can be useful as antitumoral compounds.

Scheme 1

As above mentioned, proteases are potentially involved in many diseases, including tumor growth and spreading and HIV maturation due to interaction with HIV-1 gp120 protein V3 loop [29]. Therefore, these enzymes are molecularly searched for more effective drugs that could be employed in the therapeutic. However, a notable challenge involved in the design and development of protease inhibitors has consisted to add properties as high enzymatic inhibition rates and suitable bioavailability in a single molecule [30]. Several potent peptide inhibitors are available, whereas these compounds fail to satisfy the pharmacokinetic requirements in view of high hydrophilicity and hydrolysable moieties present in their structures. Thereby, small non-peptide molecules are currently preferred to survey novel antiproteolytic drugs. In this work, we have reported the in vitro inhibition of model enzymes of cysteine and serine proteases, papain and trypsin, respectively, CatB and CatG by four benzophenones derivatives presenting lipophilic character appropriate to cross biological membranes, which would make possible the use of most active assayed benzophenones as pharmaceutical ingredients. In addition, the results obtained with flexible docking simulations have shown interesting structure-activity relationships and can be useful in the rationalizing of the anti-HIV effect presented by these compounds.

2. Chemistry

The natural polyprenylated benzophenones **1** and **3** were isolated from the ethanolic and hexanic extracts of *G. brasiliensis* dried and powdered seeds (700 g) and fruits (1000 g), respectively, whereas the compound **2** was obtained from both prior extracts. Chromatographic efforts on thin layer plates and filled columns have been employed in order to achieve the isolation of these compounds. For purification, several

recrystallizations in methanol solution were performed to give 0.51, 2.80 and 0.65 g of **1**, **2** and **3**, respectively, which were characterized by spectroscopic methods (UV, IR, MS, 1D and 2D spectra of ^{1}H and ^{13}C NMR) and their intra and inter-molecular geometries in the solid state were entirely determined and rationalized using single crystal X-ray diffraction (XRD) analysis [22,26,31,32]. More details concerning extract preparation, chromatographic conditions (solvent set used as eluent, stationary phase, supports) and fractioning (volume and numbers of collected fractions, joining of fractions according to similarity in TLC, subdivisions of fraction groups, wash steps), instrumentation general methods and data for UV, IR, MS, NMR and XRD analyses, including structural solving and refinement starting from XRD intensity measurements, can be found in three papers to be soon published [26,27,32]. As described before by us [25], the compound **4** was synthesized reacting salicylic acid and resorcinol and purified upon standing for seven days in the form of yellow needles, from which a suitably sized clear single crystal was selected for the XRD experiment [31]. The software ORTEP-3 [33] was used in the presentation of the crystal structures of the four studied benzophenones. Diphenylmethanone (benzophenone, **5**) from Merck (Darmstadt, Germany) was also used in all investigations.

In order to appraise the purity of benzophenone derivatives, some crystals of **1**, **2**, **3** and **4** were weighted (9-12 mg) and dissolved in methanol (10 mL), performing concentrated solutions that were used to give the following dilutions in methanol:acetic acid 5% pH 3.84 [40:60 v/v, initial mobile phase for High Performance Liquid Chromatography (HPLC) running]: 40.0, 10.0 and 0.5 $mg.L^{-1}$. From each previous dilution, it was injected in triplicate a volume of 20 μL (loop capacity) in the HPLC device (Shimadzu Corporation, Kyoto, Japan) equipped with two pumps (LC-10ATvp) and diode array detector (SPD-M10Avp) set at 254 nm. The analytical column was a C18 (150mm×4.6mm) with 5 μm particle size protected by a compatible guard column. The

suitable gradient was achieved using methanol:acetic acid 5% pH 3.84 (40:60 v/v) to methanol 100% in 10 min with a solvent flow rate of 1.2 mL/min at 30 °C. Prior to pumping of the mobile phase to column, the acetic acid solution and methanol were filtered under vacuum using Millipore filter and degassed separately through He sparging directly in each storage recipient. ClassVP-LC10 software was used for data collection and acquisition. The HPLC analyses of each benzophenone at the three dilutions above described have presented chromatograms with just a single strong peak. The means ± standard deviation of the percent areas in all dilutions were 98.3±1.5, 99.8±0.2, 98.6±1.1 and 96.9±0.9%, respectively for **1**, **2**, **3** and **4**.

3. Pharmacology

Benzophenone-type compounds **1-5** were tested for their potential to inhibit papain, trypsin, CatB and CatG by spectrofluorometric measurements. Enzymatic inhibition data were stated as compound concentrations to decrease 50% enzymatic activity (IC_{50} values), which have been calculated by time-course dose response curves using five inhibitor concentrations. From the same time-course experiments, the pseudo first-order rate constants for enzyme inhibition, K_{obs}, were obtained. Assays to verify the inhibition reversibility were performed in the presence of increasing substrate concentrations and by the protocol where a dithiothreitol (DTT) treatment is applied. Leupeptin (LP), chymostatin, 1-[[(L-*trans*-epoxysuccinyl)-L-leucyl]amino]-4-guanidinobutane (E-64) and soybean trypsin inhibitor (SBTI) were used as reference inhibitors in the trials of CatB, CatG, papain and trypsin, respectively.

4. Results and Discussion

As can be viewed in Table 1, a display of IC_{50} values, one of the benzophenones derivatives, the compound **1**, has avidly inhibited all assayed enzymes with different degrees of selectivity for the proteases, binding preferentially to CatG. It is important to highlight that its IC_{50} value (2.7±0.1 μM) against CatG is almost the same to that one obtained from the classical inhibitor of serine proteases, chymostatin (2.1±0.1 μM). On CatB, papain and trypsin, this last benzophenone derivative was also the most active compound, with quantitative inhibitory effects that potentiate it as antiproteolytic drug. The IC_{50} values of compound **1** on the former enzymes were 2.1±0.2, 1.9±0.1 and 9.4±0.3 μM, respectively. These data reveal that compound **1** is less active than the classical inhibitors investigated for each one of three peptidases, leupeptin for CatB (IC_{50} 0.047±0.003 μM), E-64 for papain (IC_{50} 0.047±0.004 μM) and SBTI for trypsin (IC_{50} 0.109±0.007 μM). All these three enzymes are known as trypsin-like hydrolases due to S1 specificity for both Arg and Lys basic residues, cleaving the C-N bond of substrate carbobenzyloxy-Phe-Arg-(7-amino-4-methyl-coumarin) (Z-FR-AMC) between the Arg amino acid and AMC group [34]. Although the compound **1** has strongly polarized groups as carbonyl and hydroxyl ones, anyone of its structural motifs does not resemble guanidinium and ε-amino side chains of Arg and Lys amino acids, respectively, which are required preferentially for substrate binding to enzymatic S1 site. This potential non-peptide antiproteolytic natural product evaluated in this work presents emphasized hydrophobicity, an essential structural feature that allows us to correlate the moderately high inhibitory activity of **1** on trypsin-like proteases with weak interactions occurring into S1 pocket as result of low chemical compatibility between the inhibitor and residues owning acid side groups at this site. On the other hand, CatG, a chymotrypsin-like proteinase which keeps S1 specificity for hydrophobic amino acid residues, is selectively

inhibited by the compound **1** at quite low concentrations, in agreement with its nonpolar character that favors the anchoring. Further on, a discussion more detailed relating other structural motifs of benzophenone derivatives with CatG inhibition can be found.

Table 1

The activities of **1** against all enzymes were approximately 2-69 folds higher than that manifested by compounds **2** and **3**, the other natural polyprenylated benzophenones that also inhibited significantly the four enzymes. On the other hand, the synthetic derivatives **4** and **5** were able to grow weak the enzymatic property just at high dosages. In an inhibitory concentration range similar to that described for **1** by us, the natural biflavones 2,3-dihydroamentoflavone and hinokiflavone are reported as reversible inhibitors of CatB [35]. On this point, an interesting structure-activity relationship can be stated: the capacity to inhibit the enzymatic activity increases according to number of prenyl groups attached at the diphenylmethanone moiety. With regard to CatG inhibition, the compound **1**, a pentaprenylated benzophenone, is about 14, 36 and 160 folds more active than the tetraprenylated (**2**), triprenylated (**3**) and nonprenylated (**4**) compounds, respectively**.** In agreement with this previous activity sequence, the CatG inhibitory ability of **1** is very greater than that of the nonprenylated compound **5** and the numerical ratio between quantitative inhibitions of **1** and **5** was not possible to estimate in view of the IC_{50} value of **5** to have not been established by the sensitive method employed. The approximated inhibition ratios between 1 and 2; 1 and 3; 1 and 4; 1 and 5 were respectively 35:1, 49:1, 94:1 and 138:1 for CatB; 10:1, 69:1, 364:1 and 1824:1 for papain; 2:1, 11:1, 32:1 and 368:1 for trypsin, strengthening the relationship between the prenyl group number bonded to benzophenones and their antiproteolytic properties.

Nevertheless, the natural compounds **2** and **3** have presented quite more potent antiproteolytic activity than the synthetic ones **4** and **5** (about 2-178 times). These biological differences can be explained when we compare the crystalline structures of the compounds **1-3** with **4**, once electronic and conformational features are described for all tested natural benzophenones, which are not seen in **4**. These polyprenylated compounds have a planar chelating six-membered cyclic system electronically delocalized, formed by two oxygens, where one of them is bonded to carbon bridging the substituted phenyl and bicyclic rings and another oxygen is linked to second carbon from bicycle[3.3.1]nonane moiety, a hydroxyl hydrogen atom participating of intramolecular noncovalent and covalent bonds and three carbons connecting the two oxygen atoms, where one of them is the bridge carbon and the other two are from bicycle ring, C2 and C3. The referred chelating cycle is almost entirely planar in the compounds **1-3** in view of the highest calculated deviations from the least-squares plane passing through the six cyclic atoms aforementioned to be -0.046(3) Å**,** -0.058(5) Å and -0.043(3) Å for bridge carbons of **1, 2** and **3**, respectively. However, in the compound **4**, the carbonylic C-atom has been deviated -0.135(1) Å from the better fitted least-squares plane passing through the six atoms cyclized by an intramolecular noncovalent hydrogen bond where the *ortho*-hydroxyl group from 2,4-dihydroxyphenyl moiety is the H-donor and the carbonylic oxygen is the H-acceptor, a value that is larger than we might expect for a significantly planar system. In the Figure 1, an ORTEP-3 representation [33] of the compounds **1-4,** the almost planar six-membered cyclic moiety, which is stabilized by an intramolecular noncovalent H-bond, can be clearly observed in the structures **1-3**.

Figure 1

The two phenolic hydroxyl groups of compound **1** can also play a key role in the molecular binding of **1** to enzymatic receptor site, enhancing the affinity between the respective inhibitor and macromolecules by mean of two possible interacting mechanisms: a direct one, where the aromatic OH moieties would donate and/or accept hydrogens from certain amino acid residues, likewise other dipolar, electrostatic or chelating contacts could be involved; and another indirect one, where the keto-enol tautomer of **1,** that differs of those in solid and solution states of compounds **2** and **3** and is classically rationalized with basis on electronic resonance effect offered by one of the benzene OH groups [26], would attach to proteases more strongly than otherwise a distinct tautomeric form had prevailed over one which is found. The previously mentioned keto-enol tautomeric forms of the natural benzophenones here studied were proposed by NMR spectroscopy techniques in solution-state and accurately identified by XRD analyses. The crystallographically elucidated tautomers of the compounds **1**-**3** are also shown in Figure 1. Concerning the influence of an aromatic hydroxyl group on the keto-enol tautomerism of **1**, it was verified by us that the OH group located in *para*-position from aromatic ring in relation to aromatic carbon atom attaching to the carbonyl group raises a further delocalized resonance structure passing through OH_{para}-Ph-C=O. Such electronic conjugation increases the nucleophilic character of the out-of-ring plane oxygen atom, which thereby bonds covalently to a hydrogen changeably placed in the structure that could be firmly linked to other two oxygens. To make clear, such hydrogen atom is labeled H_x in the Figure 1, and the three oxygens in which this variably positioned hydrogen could be covalently linked are bonded to C2, C4 and C10 carbons. As result, the oxygen in query, which is bonded to carbon bridging the 13,14-dihydroxylated phenyl and bicycle[3.3.1]nonane-2,4,9-trione moieties, is featured as hydroxylic one instead of carbonylic oxygen that is noted in **2** and **3**. Indeed, the tautomeric form of **1** is different of those of compounds **2** and **3** and this

dynamic feature can be crucial for detached inhibitory activity of **1** on serine and papain proteases, as it can be observed in the Figure 2, a molecular representation of compound **1** computationally docked on the active site of CatG. The hydrogen bond involving Lys217 and the hydroxyl group at C10 as hydrogen acceptor and donor [O-H10(**1**)… $O_{backbone}$(Lys217) distance is 1.856 Å], respectively, agrees with the former hypothesis concerning the influence of keto-enol tautomeric form of compound **1** to its highest antiproteolytic activity, once the hydroxyl group at C10 is sterically able to donate the hydrogen atom to backbone carbonyl group of Lys217. On the other hand, in compounds **2** and **3**, where a carbonyl moiety takes place at this position and the hydrogen atom of keto-enol six-membered cycle is covalently bonded to oxygen atom at C2, the H-bond in query between the inhibitors and CatG was not pointed out by flexible docking simulations. Specific tautomers of protease inhibitors are required for favorable interaction between anchoring groups and the amino acids of active site, such as Asp189, a critical residue for substrate/inhibitor binding to trypsin-like serine proteases [36]. Furthermore, the additional resonance effect occurring only in **1** influences several bond angles and lengths and torsional deviations in whole molecule, as the torsional angle between the bridge hydroxyl group and the least-square plane through aromatic ring. For **1**, a torsional angle of 31.1(5)° is observed, whereas for **2** and **3** these corresponding values are 37.3(7)° and 43.7(3)°, respectively. This decreased twisting for **1** can be viewed as consequence of electronic conjugation offered by 13,14-dihydroxyphenyl group in resonance with bridge hydroxyl group, which aligns the query groups. With regard to this point, another important SAR statement can be postulated: the inhibitory activity of natural benzophenones on the assayed proteases increases proportionally according to planarity enhancement between bridge hydroxyl/carbonyl and 13,14-dihydroxyphenyl/phenyl groups. After flexible docking, the torsional angle between the bridge group and the least-square plane through

aromatic ring of compounds **1** and **3**, 25.9° and 39.9°, respectively, is lower than the respective values reported by XRD analysis, which strengthens our statement regarding the relationship between planarity and inhibitory effect. On the other hand, for compound **2**, the dihedral angle in query is 40.3°, a value slightly more opened than that one measured at solid state, which is 37.3(7)°. A suitable orientation between hydrophobic motifs from enzymes and inhibitors can be the reason of the above commented planarity to be required for high inhibitory activity. Whereas the keto-enol six-membered cyclic core would anchor the inhibitor in enzyme active site by electrostatic, hydrogen and covalent (see infra) bonds, the phenyl moiety, at adequate orientation, would stack with nonpolar groups of certain amino acid residues by van der Waals, hydrophobic and π-π contacts. This hypothesis is strengthened taking in account the selective binding of compound **1** to CatG, a chymotrypsin-like protease that preferentially cleaves the peptide bond of fluorescent substrate (*ortho*-aminobenzoic acid)-AIAFFSRQ-[N-(ethylenediamine)-2,4-dinitrophenyl amide] (Abz-AIAFFSRQ-EDDnp) between two Phe residues after their benzyl side chains to be specifically recognized by S1 site in the enzyme [34,37]. At this subsite, there are two key residues, Phe191 and Glu226, pocketing the hydrophobic and polarized groups of substrate/inhibitor, respectively. The docking simulations have modeled a partial interaction of certain peptide substrate benzyl groups which do not fit completely in S1 pocket due to their unfavorable conformational features hindering sterically the phenyl stacking [37]. Putatively, the high coplanarity between the 13,14-dihydroxyphenyl and hydroxymethylene groups as consequence of further electronic resonance in the compound **1** allows the entire entry of dihydroxy-substituted phenyl group into S1 subsite of CatG by mean of thermodynamically optimized and aligned contacts between Phe191 and the inhibitor benzene moiety, as well as the 14-hydroxy aromatic substituent could contribute to overall anchoring through electrostatic bindings and hydrogen donations to Glu226,

basing the greatest in vitro antiproteolytic effect of compound **1** on CatG. These previous statements are supported by flexible docking analyses (Table 2 and Figure 2), which have shown two tight van der Waals (VDW) contacts between Phe191 and substituted phenyl ring of compound **1** [The C15(**1**)…H2'$_{ar}$(Phe191) and C16(**1**)…H3'$_{ar}$(Phe191) distances are equal to 2.28 and 2.51 Å, respectively], a hydrogen bond between Glu226 and 14-hydroxy substituent at *para*-position from phenyl ring in relation to aromatic carbon atom attaching the bridge group [O-H14(**1**)…O3'(Glu226) interaction length is 2.392 Å], and another H-bond between Gly216 and carbonyl oxygen atom at C4 [N-H$_{backbone}$(Gly216)…O4(**1**) distance measures 1.924 Å]. The contribution of the prenyl groups for compound **1** binding to CatG was also proved by docking simulations: there are various VDW contacts between CatG and the three prenyl groups including the atoms C19-C23 (four contacts, two of them performed by an unique hydrogen atom at C22 and the others were established by C22 atom), C24-C28 (twelve contacts, one of the hydrogen atoms at C28 has performed two contacts, another of them has contributed with three interactions and the carbon atom in which these two hydrogens are bonded has also participated with three VDW bonds; one hydrogen atom at C24, C24, C25 and C26 interacted one time each) and C29-C33 (five contacts, two of them performed by an unique hydrogen atom at C33 and another bond was established by a different hydrogen atom at C33; the last two interactions were done by C33 carbon atom). In addition, the theoretical binding results were highly correlated with in vitro inhibitory assays. The docking parameters are also displayed in Table 2, together with details of van der Waals and hydrogen bonds. Compound **1** showed a higher docking score, very likely due to the two hydroxyl groups interacting with CatG active site as well as additional hydrophobic contacts. Furthermore, guttiferone A (**1**) resembles the classical inhibitor of CatG, chymostatin, strengthening the idea of its selective binding to the active site residues.

Table 2

Figure 2

To check the kinetic profile of the hydrolysis inhibition by three natural benzophenone derivatives which have presented promising IC_{50} values claiming further experiments, the conversion of Z-FR-AMC into AMC was monitored during 30 minutes. As can be appraised in the Figure 3, CatB, papain and trypsin were quickly inhibited by compounds **1-3.** The proteolytic activities have already attained the minimum values within approximately five minutes of incubation using the three natural benzophenones, keeping practically constant residual enzymatic activity for whole period of kinetic assay. This rapid inhibition agrees with the restricted conformation number that can be permitted for the structures **1-3**, favoring an inhibitor directing towards binding site faster than otherwise the benzophenones might bend freely. Therefore, the interactions between the verified inhibitors and trypsin-like proteases are easily stabilized and consequently the inhibition process do not delay, as it was reported by mean of this time-dependent inhibition assay. In fact, it is important to emphasize that all conformational data may be correlated to the enzymatic inhibition results taking in account the marked presences of highly conjugated and electronically delocalized systems and noncovalent intramolecular hydrogen bonds in the benzophenone derivatives, along with a intramolecular dipolar interaction between the unsaturation of the prenyl moiety attached at C7 atom and the carbonylic oxygen bonded to fourth carbon atom of the bicycle ring which contributes to conformational stabilization (Figure 1). Such structural features have been pointed out by XRD analyses and are responsible by relatively rigid conformation of assayed compounds,

then allowing us to state structure-activity relationships based on torsional deviations between certain groups and presumed flexibility, as it can be found throughout the text.

Figure 3

The adding of increasing Z-FR-AMC concentrations to reacting mixture has not recovered the activities of trypsin and papain, enzymes which are considered as models for serine and cysteine proteases inhibition investigations, respectively, in the presence of compounds **1** and **2**, SBTI, a irreversible serine protease inhibitor under the employed analytical conditions, and E-64, a covalently bonded cysteine protease inhibitor, highlighting that the last two classical inhibitors were used as irreversible controls for each corresponding proteinase, SBTI on trypsin and E-64 on papain (Figure 4). Differently of previous findings, the inhibitory effect of compounds **3**-**5** is disappeared competitively by addition of increasing substrate concentrations. These data led us to conclude that the compounds **1** and **2** are noncompetitive inhibitors of serine and cysteine proteases, whereas compounds **3**-**5** are reversible competitive ones, accounting the much lowered inhibitory property of synthetic benzophenones **4** and **5** on both proteinase classes. The reason for reversible inhibition mode of natural compound **3** can be in its substitution pattern and conformational features: a hydrogen atom attached at the first carbon atom from bicycle moiety instead of a prenyl group like in compounds **1** and **2**, and the non-coplanarity between bridge carbonyl and phenyl groups. These structural characteristics weaken the overall interactions between compound **3** and binding site of the enzymes in comparison with the respective contacts performed by compounds **1** and **2**, culminating in the inhibitor displacement by the substrate at increasing dosages.

Figure 4

Results in keeping with the previous competitive inhibition experiment were obtained by treatment of papain-inhibitor complex with DTT, a reducing agent which can reactivate the oxidized cysteine proteases by leading catalytic Cys residue to thiol form. In this trial, the substrate hydrolysis was not restored after DTT adding where the compounds **1**, **2** and E-64 were incubated (Figure 5). In an opposed behavior, the papain was reactivated by reducing thiol DTT in the presence of benzophenones **3-5,** and the substrate cleavage degree without any inhibitor (control) was equal to that containing the compound **5** after DTT reduction. So, the inhibition of cysteine proteases by compounds **1** and **2** is irreversible, in the same way that E-64 inhibits it, and the involved mechanism is not based on oxidizing events, once DTT was not able to recover the papain hydrolytic property where these three compounds were present. Meanwhile, the enzymatic activity restoring is readily achieved by reducing procedure where the reversible inhibitors **3**-**5** take place.

Figure 5

It is known that E-64, an epoxysuccinate derivative, bonds covalently to cysteine proteases by S-alkylation of the cysteine residue in the active site [38]. In case of papain, the thiolate anion from Cys25 attacks nucleophilically the carbon atoms of the epoxide ring, which are electronically deficient, resulting in the opening of three-membered cyclic ether from inhibitor and forming a covalent thioether bond between the active site and inhibitor [38]. Other noncovalent contacts contribute for anchoring of E-64 in active site of papain. Our thought is that a similar irreversible mechanism is involved in cysteine proteases inhibition by benzophenones **1** and **2**, detaching that all above discussed

noncovalent interactions (H-bonds and van der Waals contacts) are equally important for receptor-ligand complex stabilization. The sole change is in the nucleophilic attack of cysteine residue to the carbonyl carbon atoms of compounds **1** and **2** instead of epoxidic one from E-64. As result, a thiohemiketal bond can be found in the covalently bonded complex benzophenone **1**/**2** – papain/CatB. This attack would take place at either in the second carbon atom from the bicycle moiety (compound **1**) or in the bridge carbonyl C-atom (compound **2**). We believe that these two carbonyl carbons are more susceptible to nucleophilic attack due to their highest electrophilic characters which have been verified by XRD analysis. The C=O bond lengths of corresponding carbonyl groups (1.281(4) Å for C2=O and 1.268(6) Å for C10=O in **1** and **2**, respectively) are markedly longer than the average expected value (approximately 1.22 Å), which indicate that there is an increased electronic density polarization on carbonyl double bond resulting in a pseudo-hydroxyl character of the carbonyl groups in query. Consequently, the polarization raises partial negative and positive charges around the oxygen and carbon atoms of the formed electronic dipole, respectively, potentiating the attack by nucleophiles at the partially charged carbons. As can be seen above, the carbonyl C2=O distance in **1** is larger than the C10=O length in **2**, stating the greatest electronic polarization in ketone group of **1,** which enhances the potential of nucleophilic attack on its carbon atom when compared to compound **2**. This evidence is also useful to rationalize the lowest IC_{50} values of **1** on all tested serine and cysteine proteases. Furthermore, the hypothetical reaction modeled for cysteine proteases could be also applied for CatG and trypsin inhibitions by compounds **1** and **2**, with the formation of a hemiketal derivative, once that a manner of irreversible serine proteases inhibition requires the same nucleophilic attack mechanism [38]. Several irreversible inhibitors which are nucleophilically attacked at carbonyl groups can be found

in the literature, as for instance the peptide aldehyde [39], chloromethyl ketone [40] and α,β-epoxyketone [41] derivatives.

5. Conclusion

Three natural polyprenylated benzophenone derivatives have shown potential inhibitory effect on cysteine proteases CatB and papain and serine peptidases CatG and trypsin. The pentaprenylated catecholic benzophenone guttiferone A inhibits selectively CatG at concentration similar to the peptide-based classical inhibitor of this enzyme, chymostatin, which potentiates such natural product as antiproteolytic drug for treatment of diseases in which the query protease is related, as several kinds of tumors. Its usefulness for antineoplastic therapy is further emphasized when we have accounted the beneficial effect of compounds possessing the bicycle[3.3.1]-nonanetrione moiety on tumoral and cancerous cell division. Therefore, the single natural compound adds non-peptide feature that is desired for antiproteolytic drugs with the property to act by some independent and different molecular mechanisms: altering of signal transduction pathways that results in mitosis level decreasing, inhibition of enzymes involved in DNA replication and chromosome stability, and blockage of tumor growth and dissemination by CatG and CatB activity inhibition, as it was found here. In addition, the anti-HIV ability initially reported in 1992 for compound **1** and that has been later described for compound **2** in 2005 may be based on the inhibitory activity against enzymes of protease class, once the hydrolases play an essential role in HIV maturation. Meanwhile, the synthetic benzophenones **4** and **5** have not presented significant inhibitory capacity against anyone of assayed enzymes. The natural compounds **1-3** bond quickly to cysteine and serine proteases, whereas the enzymatic inhibitions of **1** and **2** is noncompetitive, the compound **3** inhibits competitively

papain and trypsin, once its inhibitory activiy is reverted by adding substrate at increasing concentrations. Moreover, using the DTT reactivation treating we proved that the compounds **1** and **2** are irreversibly attached on papain through a putative covalent thiohemiketal bond formed by nucleophilic attack of Cys thiolate anion at a specific carbonyl carbon which is more susceptible to electronic acceptance in view of its highest positive partial charge among all carbonyl C-atoms of the inhibitors. Important SAR notes were stated and will be useful for molecular modeling and searching of novel potent benzophenone-type serine and cysteine protease inhibitors: the presences of the bicycle[3.3.1]-nonanetrione and 13,14-dihydroxy-substituted phenyl groups and keto-enol tautomeric form where the bridge carbon is hydroxylated enhance the enzymatic inhibitory activity, likewise this biological effect on serine and cysteine proteases improve according to number of prenyl groups attached at the diphenylmethanone moiety and the coplanarity between bridge hydroxyl/carbonyl and 13,14-dihydroxyphenyl/phenyl groups.

6. Experimental protocols

6.1. Chemicals

All enzymes were from Merck (Darmstadt, Germany), serine protease inhibitors SBTI and chymostatin along with cysteine ones E-64 and LP were commercially obtained from Sigma (St. Louis, USA). The fluoregenic substrates Z-FR-AMC and Abz-AFAFFSRQ-EDDnp were generously given by Dr. Luiz Juliano (Department of Biophysics, Federal University of São Paulo, Brazil). Substrate hydrolyses were monitored in a spectrofluorometer Shimadzu RF-1501 (Shimadzu Corporation, Kyoto, Japan) and the

enzymatic molar concentrations were estimated by titration according to kinetic parameters [34].

6.2. Inhibition assays

CatB inhibition experiment was performed as previously described [34], using the fluorogenic substrate Z-FR-AMC, whose hydrolysis was spectrofluorometrically measured at 460 nm after the free AMC to have been excited at 380 nm. AMC solutions were used as working standards to generate a calibration curve and the substrate has been prepared diluting several times a stock solution at 1 mg *per* milliliter of water:dimethylformamide (50:50 v/v) in the CatB buffer composed by Tris-HCl 50 mM (pH 7.5) and ethylenediaminetetraacetic acid (EDTA) 5 mM. For the tested inhibitors, each benzophenone was dissolved in dimethyl sulfoxide (DMSO) and diluted with enzymatic buffer (0.5-280 μM). These solutions were added to the buffer containing the respective enzyme previously treated with DTT 10 mM, and the resulting mixture was incubated for 5 min at isothermal 25 °C on spectrofluorometer. The enzymatic reaction was started by adding of fluorescent substrate solution at 5.2 μM to the cuvette. The final concentration of CatB in the reactant mixture was 1.0 nM and LP was used as classical inhibitor of this protease. The same laboratorial protocol was adopted for the assays with papain, trypsin and CatG, with some different experimental parameters as follow. Papain: buffer composed by sodium phosphate 50 mM (pH 6.8) and EDTA 1.0 mM, Z-FR-AMC fluorescent substrate solution was 3.1 μM, final enzymatic concentration was 7.8 nM, E-64 was used as classical inhibitor; Trypsin: buffer composed by Tris-HCl 50 mM (pH 7.5) and $CaCl_2$ 10 mM, Z-FR-AMC fluorescent substrate solution was 3.1 μM, final enzymatic concentration was 56.1 nM, SBTI was used as classical inhibitor; CatG [37]: Hepes buffer

50 mM (pH 7.4) containing NaCl 50 mM, the solution concentration of an internally quenched fluorogenic peptide Abz-AIAFFSRQ-EDDnp, where Abz is the fluorescent donor and EDDnp is the fluorescent quencher (emission and excitation wavelengths for Abz were λ_{em} = 420 nm and λ_{ex} = 320 nm, respectively), was 1.7 μM, which was spectrally computed through electromagnetic absorption of 2,4-dinitrophenyl moiety, benzophenones concentration ranging from 0.5 μM to 240 μM, final enzymatic concentration was 9.9 nM, chymostatin was used as classical inhibitor. For serine proteases trypsin and CatG, the initial treatment with DTT has not been applied.

6.3. Kinetic profile of inhibitions

To obtain the kinetic profile of the enzymatic inhibitions, the same procedure was performed for CatB, papain and trypsin using the buffers of each protease and fixed concentrations of benzophenones **1**-**3**. The fluorescent emissions originating from peptide substrate hydrolyses were quantified at 0, 2min30s, 5, 10, 20 and 30 min after the adding of Z-FR-AMC to newly incubated cuvette (1 mL) already containing the enzymes and inhibitors diluted in the respective buffers. For this trial, the final enzyme and inhibitor concentrations and added Z-FR-AMC solutions were respectively 2 nM, 15 μM and 5 μM for CatB; 3.5 nM, 9 μM and 3.1 μM for papain; and 19 nM, 10 μM and 10 μM for trypsin.

6.4. Reversibility evaluation

In order to recognize whether the benzophenone derivatives could bond either irreversibly or reversibly to the enzyme active site, papain and trypsin, models for cysteine and serine proteases, respectively, were also competitively inhibited by the compounds **1**-**5**

at 50 μM in the presence of increasing Z-FR-AMC concentrations (3.1-15.5 μM). E-64 (0.2 μM) and SBTI (0.72 μM) were comparatively used in the assays of papain (8.0 nM) and trypsin (56 nM), respectively. Furthermore, the reversibility of papain inhibition was evaluated by fluorescence measurement of a reaction mixture with either the benzophenones (50 μM) or E-64 (0.5 μM) and that has been added to it a DTT solution at 10 mM for enzymatic reactivation in case of inhibition to be reversibly based. These tests were matched with one which inhibitor was absent, and all trials were begun when the Z -FR-AMC solution (3.1 μM) has been joined to mixtures with or without DTT.

6.5. Computational docking

The GOLD program (version 3.1.1) [42] has been used and the default parameters were set: population size 100, selection-pressure 1.1, number of operations 100,000, number of islands 5, niche size 2, docking runs 5 and operator weights for migrate, mutate and crossover were 10, 95 and 95, respectively. The binding site of compounds **1**-**3** was defined as all the residues within 10 Å from one of the carboxylate oxygens of Glu226. The GoldScore fitness function was selected for scoring the docking poses. The coordinates for cathepsin G, where the complexed succinyl-Val-Pro-Phe^{P}-$(Oph)_2$ inhibitor (Oph_2 is a diphenyl ester) was first removed, from Brookhaven Protein Data Bank (PDB code 1cgh) were downloaded [43]. For compounds **1**-**3**, the geometries determined by the X-ray diffraction analysis were used as input without further optimization. Early run terminations with only three chromosomes were not reached in all simulations.

7. Acknowledgements

We thank the Brazilian Research Council CNPq (Conselho Nacional de Desenvolvimento Científico e Tecnológico) and CAPES (Coordenação de Aperfeiçoamento de Pessoal de Nível Superior) for research fellowships (ACD and FTM), FAPEMIG (Fundação de Amparo à Pesquisa do Estado de Minas Gerais Proc.: EDT-3310/06) and FINEP (Financiadora de Estudos e Projetos – Proc.: 1110/06) for financial support.

8. References

[1] K. Brocklehurst, F. Willenbrock, E. Salih, in: A. Neuberger, K. Brocklehurst (Eds.), New Comprehensive Biochemistry, Elsevier, Amsterdam, 1987, pp. 39-158.

[2] T. Taniguchi, T. Mizuochi, T. Towatari, N. Katunuma, A. Kobata, J. Biochem. 97 (1985) 973-976.

[3] H. Kirschke, A. Barret, in: B. Glaumann (Ed), Lysosomes: Their Roles in Protein Breakdown, Academic Press, London, 1987, pp. 193-238.

[4] A. Barrett, Biochem. J. 131 (1973) 809-822.

[5] J. Mort, A. Recklies, Biochem. J. 233 (1986) 57-63.

[6] L. Polgar, C. Csoma, J. Biol. Chem. 262 (1987) 14448-14453.

[7] B.E. Cathers, C. Barret, J.T. Palmer, R.M. Rydzewski, Bioorg. Chem. 30 (2002) 264-275.

[8] J.E. Koblonski, B.F. Ahram, B.F. Sloane, Ciln. Chim. Acta 291 (2000) 113-135.

[9] M. Baggiolini, U. Bretz, B. Dewald, M.E. Feigenson, Agents Actions 8 (1978) 3-10.

[10] A.J. Barrett, Methods Enzymol. 80 (1981) 561-565.

[11] W. Watorek, D. Farley, G. Salvesen, J. Travis, Adv. Exp. Med. Biol. 240 (1988) 23-31.

[12] J.G. Bieth, in: R.P. Mecham (Ed.), Biology of the Extracellular Matrix, Academic Press, New York, 1986, pp. 217-320.

[13] C.A. LaRosa, M.J. Rohrer, S.E. Benoit, L.J. Rodino, M.R. Barnard, A.D. Michelson, J. Vasc. Surg. 19 (1994) 306-318.

[14] O. Chertov, H. Ueda, L.L. Xu, K. Tani, W.J. Murphy, J.M. Wang, O.M. Howard, T.J. Sayers, J.J. Oppenheim, J. Exp. Med. 186 (1997) 739-747.

[15] T. Yamazaki, Y. Aoki, Immunology 93 (1998) 115-121.

[16] M. Padrines, M. Wolf, A. Walz, M. Baggiolini, FEBS Lett. 352 (1994) 231-235.

[17] C.M. Maison, C.L. Villiers, M.G. Colomb, J. Immunol. 147 (1991) 921-926.

[18] D.H. Allen, P.B. Tracy, J. Biol. Chem. 270 (1995) 1408-1415.

[19] S. Yui, K. Tomita, T. Kudo, S. Ando, M. Yamazaki, Cancer Sci. 96 (2005) 560-570.

[20] R.J. Beynon, J.S. Bond (Eds.), Proteolytic enzymes: a practical approach, Oxford University, Liverpool,1989.

[21] K.R. Gustafson, J.W. Blunt, H.G.M. Munro, R.W. Fuller, C.T. McKee, J.H. Cardellina, J.B. McMahon, G.M. Cragg, M.R. Boyd, Tetrahedron 48 (1992) 10093-10102.

[22] M.H. Santos, N.L. Speziali, T.J. Nagem, T.T. Oliveira, Acta. Crystallogr. C54 (1998) 1990-1992.

[23] A.J. Cruz, V.S. Lemos, M.H. Santos, T.J. Nagem, S.F. Cortes, Phytomedicine 13 (2006) 442-445.

[24] A.L. Piccinelli, O.C. Rubio, M.B. Chica, N. Mahmood, B. Pagano, M. Pavone, V. Barone, L. Rastrelli, Tetrahedron 61 (2005) 8206-8211.

[25] A.C. Doriguetto, F.T. Martins, J.A. Ellena, R. Salloum, M.H. Santos, M.E.C. Moreira, J.M. Schneedorf, T.J. Nagem, Chem. Biodiversity 4 (2007) 488-499.

[26] F.T. Martins, J.W. Cruz JR., P.B.M.C. Derogis, M.H. Santos, M P. Veloso, J.A. Ellena, A.C. Doriguetto, J. Braz. Chem. Soc. in press (2007).

[27] P.B.M.C. Derogis, F.T. Martins, T.C. Souza, M.E.C. Moreira, J.D. Souza Filho, A.C. Doriguetto, K.R. Souza, M.P. Veloso, M.H. Santos, Magn. Reson. Chem. in press (2007).

[28] D.D. Carballo, S. Seeber, D. Strumberg, R.A. Hilger, Int. J. Clin. Pharm. Th. 41 (2003) 622-623.

[29] L.E. Avril, M.D.M. Ferrer, M.B. Bourdet, F. Gauthier, FEBS Lett. 367 (1995) 251-256.

[30] M.A. Navia, P.R. Chaturvedi, Drug Discov. Today 1 (1996) 179-189.

[31] Supplementary crystallographic data sets (excluding structure factors) for compounds **1**, **2**, **3** and **4** are available through the Cambridge Structural Data Base, deposition codes CCDC 643597, IUCr DA1009, CCDC 667556 and CCDC 606243, respectively. Copies of this information may be obtained free of charge from The Director, CCDC, 12 Union Road, Cambridge, CB2 1EZ, UK (fax: +44123-336-033; e-mail: deposit@ccdc.cam.ac.uk or http:www.ccdc.ac.uk)

[32] F.T. Martins, I. Camps, A.C. Doriguetto, M.H. Santos, J. Ellena, L.C.A. Barbosa, J. Mol. Struct. submitted (2007).

[33] L.J. Farrugia, J. Appl. Cryst. 30 (1997) 565.

[34] R.L. Melo, L.C. Alves, E.D. Nery, L. Juliano, M.A. Juliano, Anal. Biochem. 293 (2001) 71–77.

[35] G.Z. Zeng, X.L. Pan, N.H. Tan, J. Xiong, Y.M. Zhang, Eur. J. Med. Chem. 41 (2006) 1247-1252.

[36] B.W. Clare, A. Scozzafava, C.T. Supuran, J. Enzyme Inhib. 16 (2001) 1-13.

[37] S. Réhault, M.B. Bourdet, M.A. Juliano, L. Juliano, F. Gauthier, T. Moreau, J. Biol. Chem. 274 (1999) 13810–13817.

[38] J.C. Powers, J.L. Asgian, O.D. Ekici, K.E. James, Chem. Rev. 102 (2002) 4639-4750.

[39] T. Sasaki, M. Kishi, M. Saito, T. Tanaka, N. Higuchi, E. Kominami, N. Katunuma, T. Murachi, J. Enzyme Inhib. 3 (1990) 195-201.

[40] T. Sasaki, T. Kikuchi, I. Fukui, T. Murachi, J. Biochem. 99 (1986) 173-179.

[41] Y. Koguchi, J. Kohno, S. Suzuki, M. Nishio, K. Takahashi, T. Ohnuki, S. Komatsubara, J. Antiobiot. 52 (1999) 1069-1076.

[42] GOLD, version 3.1.1, Cambridge Crystallographic Data Centre, Cambridge, U.K.

[43] P. Hof, I. Mayr, R. Huber, E. Korzus, J. Potempa, J. Travis, J.C. Powers, W. Bode, EMBO J. 15 (1996) 5481-5491.

Figure 1. An ORTEP [33] view of crystallographically determined structures of three natural polyprenylated benzophenones guttiferone A (**1**), epiclusianone (**2**) and garciniaphenone (**3**) together with the synthetically yielded benzophenone-type derivative 2,2',4-trihydroxybenzophenone (**4**) where an arbitrary atom labeling is displayed. Ellipsoids represent 50% probability level. Double dotted line represents either the intramolecular noncovalent hydrogen bond or the dipolar interaction between the unsaturation of the prenyl moiety attached at C7 atom and the carbonylic oxygen bonded to fourth carbon atom of the bicycle ring. The C-H H-atoms were omitted for clarity and the hydrogen atom that can be changeably placed in the structures **1**-**3** is labeled H_x and it was accurately located in each natural benzophenone using residual density maps obtained by difference Fourier synthesis during the single crystal XRD analyses [25,26,32].

Figure 2. Best docking orientation for compound **1** inside the active site of Cathepsin G. a. A full view of complex inhibitor-CatG. *b*. The hydrogen bonds that contribute for inhibitor anchoring are shown as white lines. Phe191 and Glu226 side chains were highlighted due to their key roles in the binding of inhibitor. Gly216 and Lys217 side chains are not displayed in the illustration, once the H-bonded groups of these amino acids are in the peptide chain backbone (α-amino and carbonyl groups from Gly216 and Lys217, respectively). The C-H H-atoms were omitted for clarity.

Figure 3. Kinetic profile at 25ºC of Cathepsin B, papain and trypsin inhibitions by natural polyprenylated benzophenones. The final enzyme and inhibitor concentrations and added Z-FR-AMC solutions were respectively 2 nM, 15 μM and 5 μM for CatB (buffer Tris-HCl 50 mM pH 7.5 and EDTA 5 mM); 3.5 nM, 9 μM and 3.1 μM for papain (buffer sodium phosphate 50 mM pH 6.8 and EDTA 1.0 mM); and 19 nM, 10 μM and 10 μM for trypsin

(buffer Tris-HCl 50 mM pH 7.5 and $CaCl_2$ 10 mM). Each value represents the mean ± s.e.m. of three independent assays.

Figure 4. Reversibility assay for papain and trypsin inhibitions by benzophenone derivatives with increasing substrate concentrations. Assayed concentrations: inhibiting benzophenones (50 μM), substrate Z-FR-AMC (3.1-15.5 μM, addition after 5 min of incubation at 25ºC), E-64 (0.2 μM) for papain (8.0 nM, buffer sodium phosphate 50 mM pH 6.8 and EDTA 1.0 mM), SBTI (0.72 μM) for trypsin (56 nM, buffer Tris-HCl 50 mM pH 7.5 and $CaCl_2$ 10 mM). Each value represents the mean ± s.e.m. of three independent assays.

Figure 5. Reversibility assay for papain inhibition by benzophenone derivatives after dithiothreitol (DTT) treatment. Evaluated concentrations: inhibiting benzophenones (50 μM), substrate Z-FR-AMC (3.1 μM), E-64 (0.5 μM), newly activated papain (8.0 nM, buffer sodium phosphate 50 mM pH 6.8 and EDTA 1.0 mM). A DTT solution (10 mM) was added to a reacting mixture already containing the inhibitor and the fluorescence value was measured in the moment when the substrate was joined. Control: without inhibitor. The clustered columns, which represent the mean of three independent assays, lead the upper error bars (s.e.m.).

Scheme 1. Chemical structures of benzophenones guttiferone A (**1**), epiclusianone (**2**), garciniaphenone (**3**), 2,2',4-trihydroxybenzophenone (**4**) and diphenylmethanone (**5**).

Table 1. Quantitative in vitro inhibitory effect of natural and synthetic benzophenone derivatives on cysteine proteases Cathepsin B (CatB) and papain and serine peptidases Cathepsin G (CatG) and trypsin.

Compound	IC_{50} values (μM) [a]			
	CatB	Papain	CatG	Trypsin
guttiferone A (**1**)	2.1±0.2	1.9±0.1	2.7±0.1	9.4±0.3
epiclusianone (**2**)	73.7±5.8	19.5±1.8	37.9±2.1	20.1±1.7
garciniaphenone (**3**)	103.5±4.4	130.8±4.8	97.6±5.2	103.5±8.5
2,2',4-trihydroxybenzophenone (**4**)	198.0±10.7	693.1±63.0	433.2±25.5	301.4±7.7
benzophenone (**5**)	288.8±22.2	3465±693	ND [b]	3466±315
Leupeptin (LP) [c]	0.047±0.003			
E-64		0.047±0.004		
Chymostatin			2.1±0.1	
SBTI				0.109±0.007

[a] Each IC_{50} value represents the mean ± standard deviation of triplicates and the analytical and reacting conditions can be found in the experimental part. [b] ND: IC_{50} value was not established by the sensitive method employed. [c] The compounds LP, E-64, chymostatin and SBTI were used as reference inhibitors of the corresponding proteases where they have been assayed.

Table 2. Distances of van der Waals contacts and hydrogen bonds in the CatG-compound **1** complex and the docking parameter of three natural polyprenylated benzophenones on CatG.

*CatG-compound **1** van der Waals contacts* [a]		
atom of compound **1**	amino acid residue of CatG	distance (Å)
H10	Lys217	2.591
H17a	Ser218	1.339
H17a	Ser218	2.420
H33b	Lys192	1.849
H33c	Lys192	1.116
H33c	Lys192	2.105
H24a	Gly216	1.801
H28a	Phe172	1.700
H28a	Phe172	2.529
H28b	Gly216	2.147
H28b	Gly216	2.413
H28b	Phe172	1.675
H22b	Hip57	2.196
H22b	Hip57	2.583
C16	Phe191	2.512
C15	Phe191	2.280
C13	Tyr215	2.556
C17	Ser218	2.073
C17	Ser218	3.151
C33	Lys192	1.771
C33	Lys192	2.804
C24	Gly216	2.535
C25	Lys217	2.439
C26	Lys217	2.282
C28	Phe172	1.928
C28	Phe172	2.946
C28	Gly216	2.906
C22	Hip57	2.988
C22	Hip57	3.035
O2	Ser218	1.955
O2	Ser218	2.614
O2	Ser218	2.281
O2	Ser218	2.672
O10	Ser218	1.911
O10	Ser218	2.931
O4	Tyr215	1.807
O4	Tyr215	2.806
*CatG-compound **1** hydrogen bonds*		
hydrogen donor	hydrogen acceptor	distance (Å)
N-$H_{backbone}$(Gly216)	O4(**1**)	1.924
O-H10(**1**)	$O_{backbone}$(Lys217)	1.856
O-H14(**1**)	O3'(Glu226)	2.392

CatG-inhibitor docking score [b]		
compound **1**	compound **2**	compound **3**
-6.15	-6.65	-6.52

[a] The letters a, b and c label different hydrogen atoms bonded to a same carbon. [b] Higher docking scores correlate more favorable binding between inhibitor and enzyme.

Figure 1

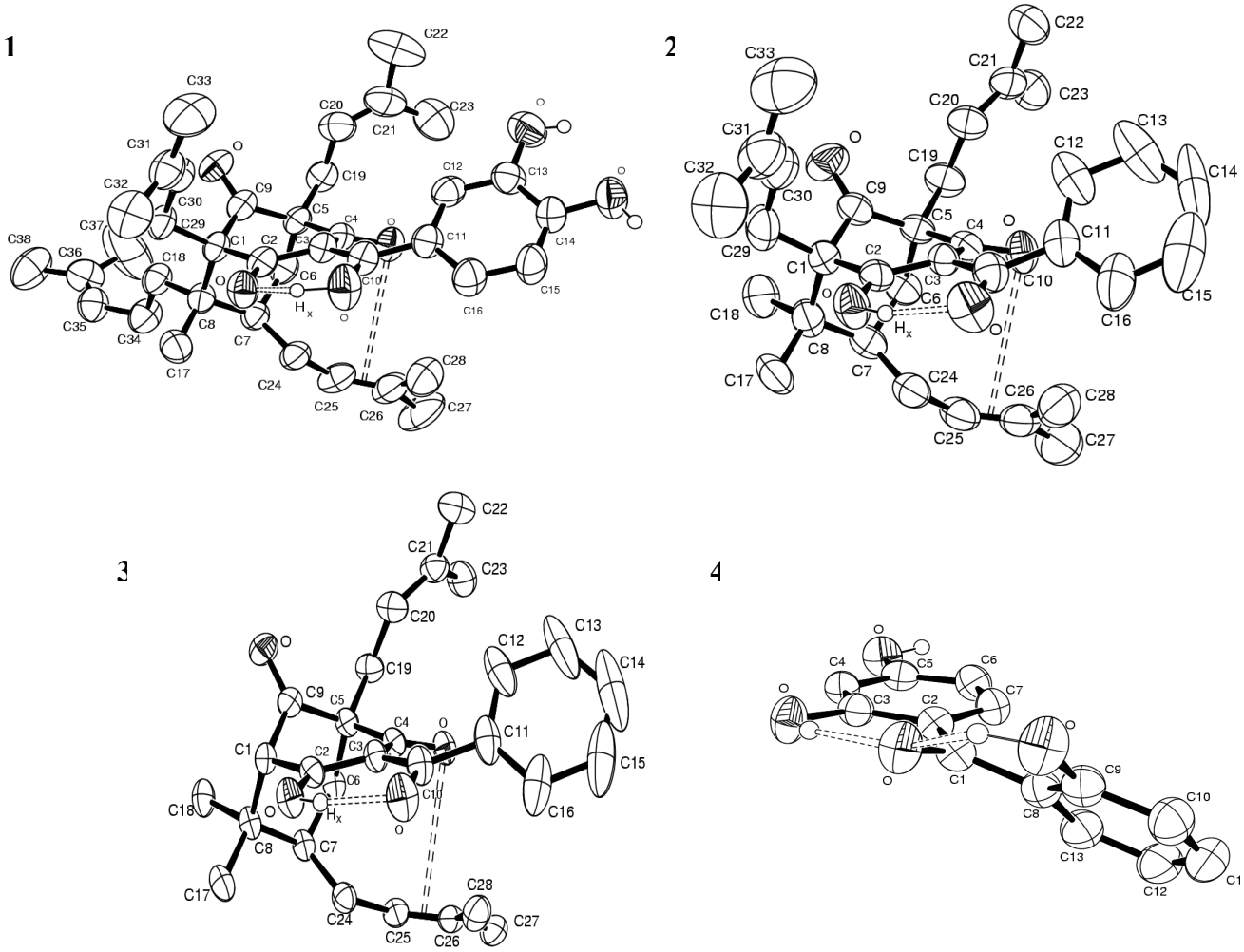

Figure 2

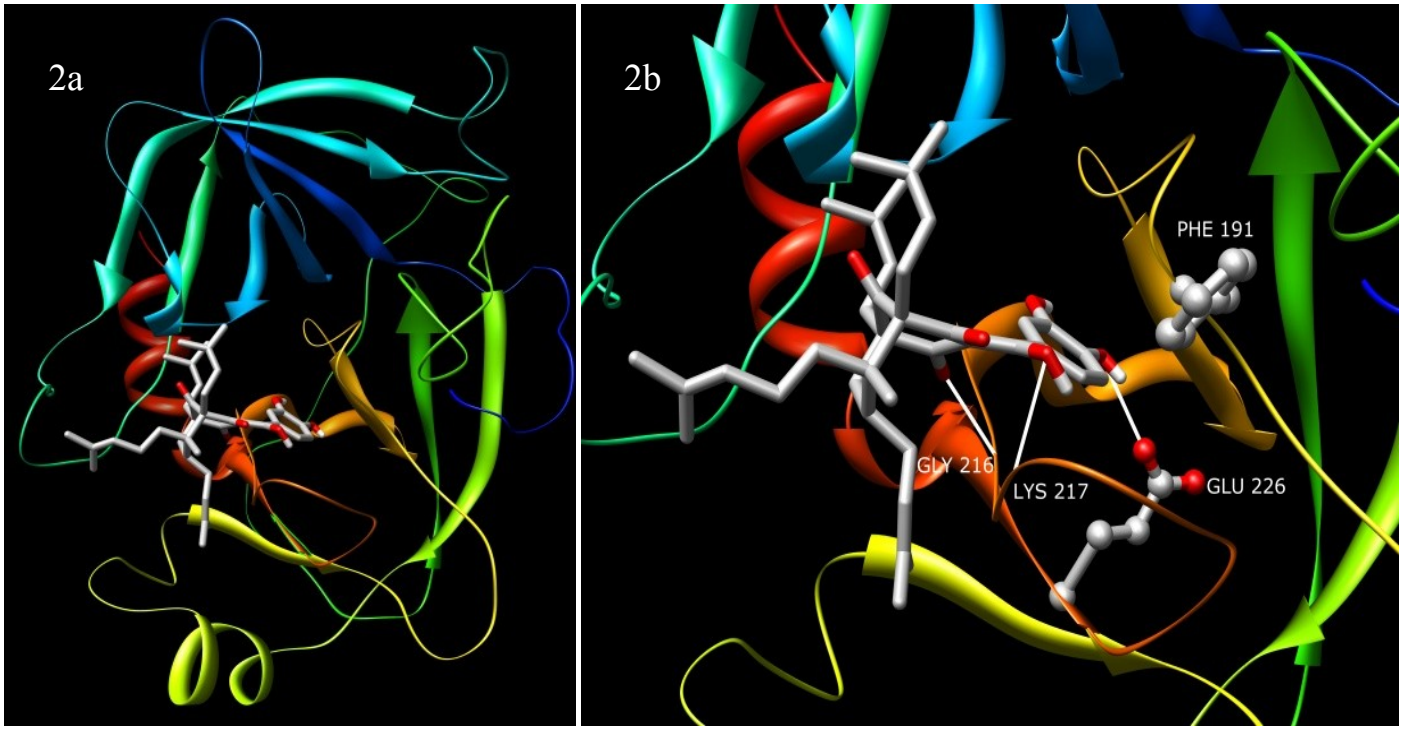

Figure 3

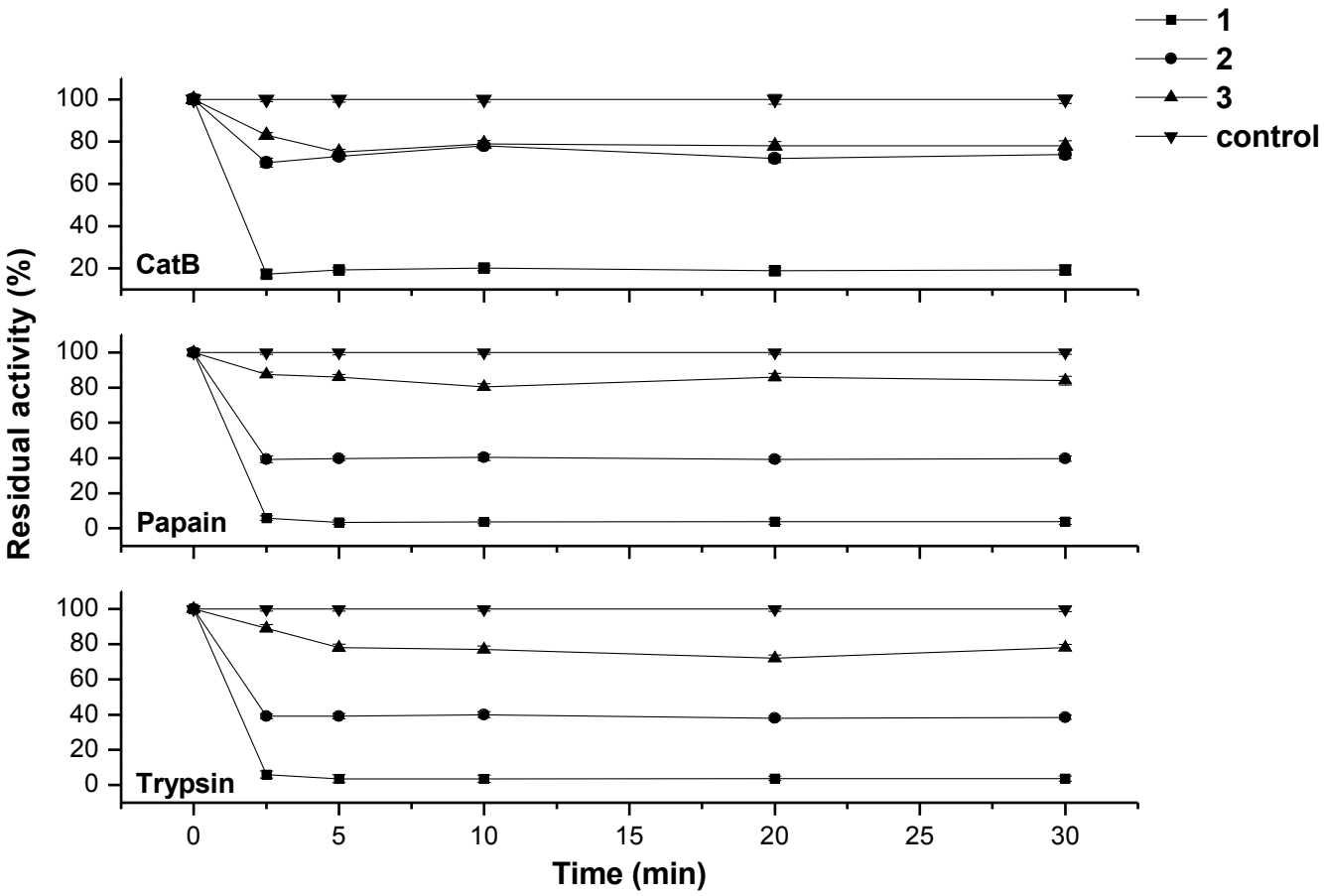
1
2
3
control
Residual activity (%)
CatB
Papain
Trypsin
Time (min)
0
5
10
15
20
25
30
20
40
60
80
100

Figure 4

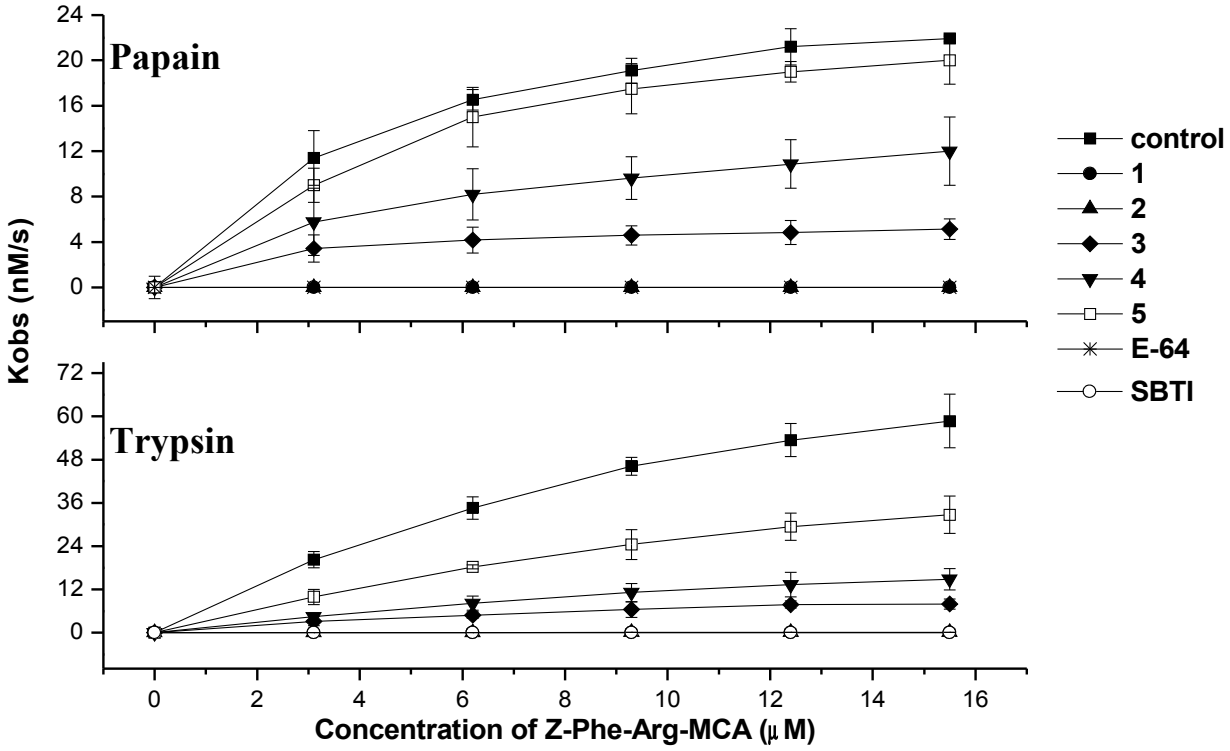
Papain
Trypsin
Kobs (nM/s)
Concentration of Z-Phe-Arg-MCA (μM)
control
1
2
3
4
5
E-64
SBTI

Figure 5

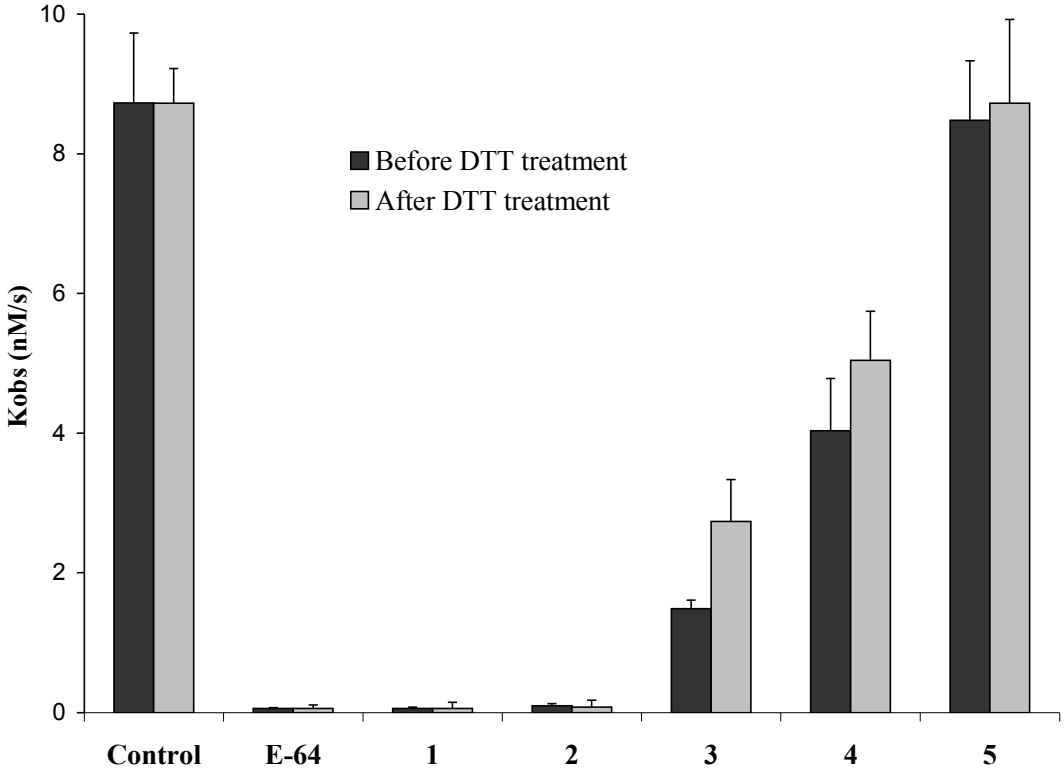
10
8
6
4
2
0
Kobs (nM/s)
Before DTT treatment
After DTT treatment
Control
E-64
1
2
3
4
5

Scheme 1

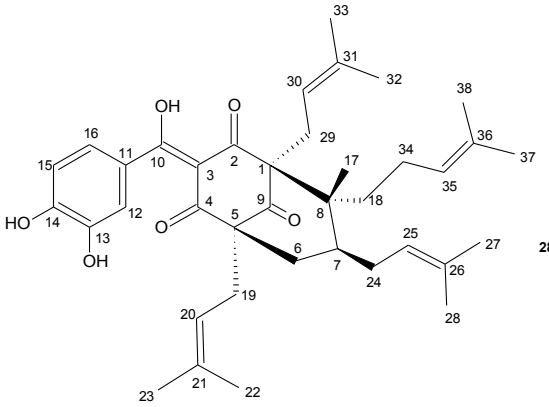

1

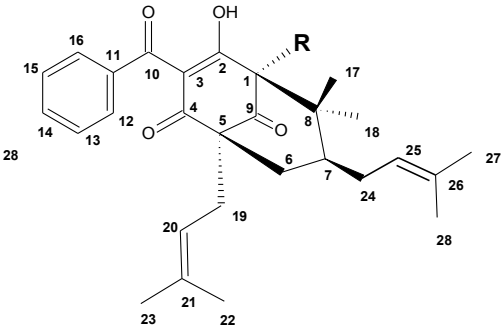

2, **R =**

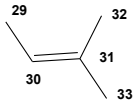

3, **R =** **H**

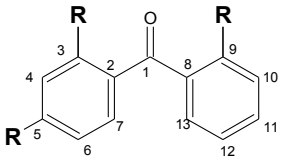

4, **R =** **OH**

5, **R =** **H**

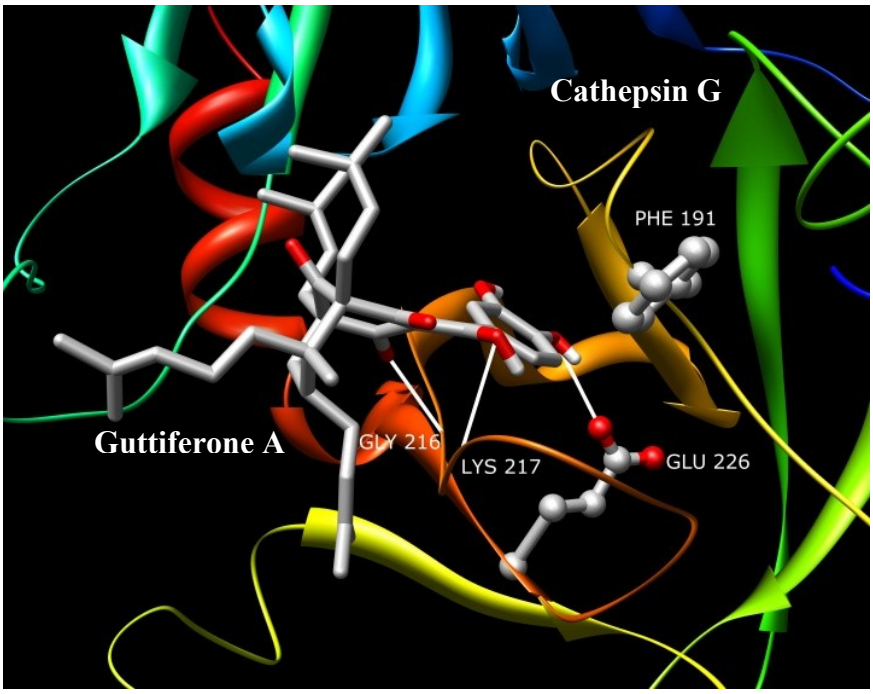

GRAPHICAL ABSTRACT

5 PRODUÇÃO BIBLIOGRÁFICA RELEVANTE

5.1 ARTIGOS

1. MARTINS, F. T., SANTOS, M. H., NEVES, P. P., BARBOSA, L. C. A., DORIGUETTO, A. C. A simple and direct qualitative method for polyprenylated benzophenones detection in extracts from *Garcinia brasiliensis* Mart. using X-ray powder diffraction patterns. **Journal of Natural Products**. in preparation, 2007.

2. PEREIRA, F. J., POLO, M., MARTINS, F. T., MOREIRA, M. E. C., COSTA, A. M. D. D., BARBOSA, L. C. A. Composição química e atividade antiinflamatória do óleo essencial do pericarpo de *Copaifera langsdorffii* desf. **Acta Farmacéutica Bonaerense.** in preparation, 2007

3. SANTOS, M. H., MÉGDA, J., CRUZ, P. B. M., MARTINS, F. T., MOREIRA, M. E. C. An inexpensive plate coater equipment of stationary phase for thin-layer chromatography. **Química Nova**. 30: 1747-1749, 2007.

4. MARTINS, F. T., POLO, M. Anatomical and molecular features of *Hyptis suaveolens* (L.) Poit. reproductive development: relationships among photoperiod, meristem cell density and expression pattern of a putative Arabidopsis gene LEAFY homolog. **Revista Brasileira de Botânica**. in press, 2007.

5. DEROGIS, P. B. M. C., MARTINS, F. T., SOUZA, T. C., MOREIRA, M. E. C., SOUZA FILHO, J. D., DORIGUETTO, A. C., SOUZA, K. R., VELOSO, M. P., SANTOS, M. H. Complete assignment of the 1H and 13C NMR spectra of garciniaphenone and keto-enol equilibrium statements for prenylated benzophenones. **Magnetic Resonance in Chemistry**. 46: 278-282, 2008.

6. MARTINS, F. T., DORIGUETTO, A. C., SOUZA, T. C., SOUZA, K. R., SANTOS, M. H., MOREIRA, M. E. C., BARBOSA, L. C. A. Composition, anti-inflammatory and antioxidant activities of the volatile oil from *Garcinia brasiliensis* Mart. fruit peel. **Chemistry & Biodiversity**. in press , 2007.

7. DORIGUETTO, A. C., NEVES, P. P., MARTINS, F. T., MASTELARO, V. R., MASCARENHAS, Y. P., EIRAS, J. A., LENTE, M. H. Long-Range order structure in Pb1¡xLaxTiO3 ceramics below and above of ferroelectric phase. **Activity Reports of Brazilian Synchrotron Light Laboratory**, 2007.

8. MARTINS, F. T., SANTOS, M. H., POLO, M., BARBOSA, L. C. A. Effects of the interactions among macronutrients, plant age and photoperiod in the composition of *Hyptis suaveolens* (L.) Poit essential oil from Alfenas (MG), Brazil. **Flavour and Fragrance Journal.** 22: 123-129, 2007.

9. MARTINS, F. T., CAMPS, I., NEVES, P. P., DORIGUETTO, A. C., SANTOS, M. H., ELLENA, J., BARBOSA, L. C. A. Garciniaphenone, a novel natural polyprenylated benzophenone from *Garcinia brasiliensis*. **Journal of Molecular Structure.** submitted, 2008.

10. MARTINS, F. T., ASSIS, D. M., SANTOS, M. H., CAMPS, I., VELOSO, M. P., JULIANO, M. A., ALVES, L. C., DORIGUETTO, A. C. Natural polyprenylated benzophenones inhibiting cysteine and serine proteases. **European Journal of Medicinal Chemistry.** submitted, 2008.

11. MARTINS, F. T., CRUZ JUNIOR, J. W., DEROGIS, P. B. M. C., SANTOS, M. H., VELOSO, M. P., ELLENA, J., DORIGUETTO, A. C. Natural polyprenylated benzophenones: keto-enol tautomerism and stereochemistry. **Journal of the Brazilian Chemical Society.** 18: 1515- 1523, 2007.

12. DORIGUETTO, A. C., MARTINS, F. T., ELLENA, J., SALLOUM, R., SANTOS, M. H., MOREIRA, M. E. C., SCHNEEDORF, J. M., NAGEM, T. J. 2,2',4-Trihydroxybenzophenone: crystal structure and anti-inflammatory and antioxidant activities. **Chemistry & Biodiversity.** 4: 488 - 499, 2007.

13. MARTINS, F. T., SANTOS, M. H., POLO, M., BARBOSA, L. C. A. Chemical variation in the essential oil of Hyptis suaveolens (L.) Poit., under cultivation condition. **Química Nova.** 29:1203 - 1209, 2006.

5.2 CAPÍTULO DE LIVRO

1. BARBOSA, L. C. A., MARTINS, F. T., TEIXEIRA, R. R., POLO, M. Chemical variability and biological activities of volatile oils from *Hyptis suaveolens*. In: **Biodiversity and Conservation of Medicinal and Aromatic Plants**, Thangadurai, D. (Ed.). New Delhi, Bioscience Publications, 2007.

5.3 APRESENTAÇÃO ORAL DE TRABALHO

1. MARTINS, F. T., CRUZ JUNIOR, J. W., DEROGIS, P. B. M. C., SANTOS, M. H., VELOSO, M. P., ELLENA, J., DORIGUETTO, A. C. Keto-enol tautomerism and stereochemical relationships in natural prenylated benzophenones based on their XRD crystal structures. II **Workshop da Pós-Graduação – XIII Jornada de Iniciação Científica de Alfenas**, Universidade Federal de Alfenas, Alfenas, 2007.

APÊNDICE I

Artigo acerca da estrutura cristalina e atividades antioxidante e antiinflamatória de 2,2',4-triidroxibenzofenona, uma benzofenona sintética empregada nos ensaios de inibição enzimática descritos na Parte 2. Este trabalho foi realizado paralelamente àqueles descritos nas Partes 1 e 2, e é apresentado nesta seção devido à sua relevância para compreensão das relações estruturais envolvidas na habilidade anti-proteolítica das benzofenonas.

APÊNDICE II

Artigo acerca da composição e atividades antiinflamatória e antioxidante do óleo volátil extraído da casca do fruto da mesma espécie vegetal alvo de estudos fitoquímicos apresentados nesta dissertação. Este trabalho é apresentado nesta seção devido à sua contribuição significativa para a caracterização química de *Rheedia brasiliensis* e por expor a aplicação potencial de outros constituintes desta planta, que não apenas os derivados benzofenônicos, como fitoterápicos.